Unprecedented spring 2020 ozone depletion in the context of 20 years of measurements at Eureka, Canada

Kristof Bognar[1,1], Ramina Alwarda[1,1], Kimberly Strong[1,1], Martyn P. Chipperfield[2,2], Sandip Dhomse[2], James Drummond[3,3], Wuhu Feng[2,2], Vitali Fioletov[4,4], Florence Goutail[5,5], Beatriz Herrera[1,1], Gloria L Manney[6,6], Emily M. McCullough[7,7], Luis Millan[8,8], Andrea Pazmino[9,9], Kaley A. Walker[1,1], Tyler Wizenberg[1,1], Xiaoyi Zhao[10,10], and Sandip Dhomse[2]

[1]University of Toronto
[2]University of Leeds
[3]Dalhousie University
[4]Environment Canada
[5]Centre national de la recherche scientifique
[6]Northwest Research Associates
[7]Department of Physics and Atmospheric Science, Dalhousie University
[8]Jet propulsion laboratory
[9]LATMOS - CNRS
[10]Envionment and Climate Change Canada

November 30, 2022

Abstract

In the winter and spring of 2019/2020, the unusually cold, strong, and stable polar vortex created favorable conditions for ozone depletion in the Arctic. Chemical ozone loss started earlier than in any previous year in the satellite era, and continued until the end of March, resulting in the unprecedented reduction of the ozone column. The vortex was located above the Polar Environment Atmospheric Research Laboratory in Eureka, Canada (80 °N, 86 °W) from late February to the end of April, presenting an excellent opportunity to examine ozone loss from a single ground station. Measurements from a suite of instruments show that total column ozone in 2020 was at an all-time low in the 20-year dataset, 22 to 102 DU below previous records set in 2011. Ozone minima (<200 DU), enhanced OClO and BrO slant columns, and unusually low HCl, $ClONO_2$, and HNO_3 columns were observed in March. Polar stratospheric clouds were present as late as 20 March, and ozonesondes show unprecedented depletion in the March and April ozone profiles (to <0.2 ppmv). While both chemical and dynamical factors lead to reduced ozone when the vortex is cold, the contribution of chemical depletion was exceptional in spring 2020 when compared to typical Arctic winters. The mean chemical ozone loss over Eureka was estimated to be 111-127 DU (27-31%) using April measurements and passive ozone from the SLIMCAT chemical transport model. While absolute ozone loss was generally smaller in 2020 than in 2011, percentage ozone loss was greater in 2020.

Unprecedented spring 2020 ozone depletion in the context of 20 years of measurements at Eureka, Canada

Kristof Bognar[1], Ramina Alwarda[1], Kimberly Strong[1], Martyn P. Chipperfield[2,3], Sandip S. Dhomse[2,3], James R. Drummond[4], Wuhu Feng[2,5], Vitali Fioletov[6], Florence Goutail[7], Beatriz Herrera[1], Gloria L. Manney[8,9], Emily M. McCullough[4], Luis F. Millán[10], Andrea Pazmino[7], Kaley A. Walker[1], Tyler Wizenberg[1], Xiaoyi Zhao[6]

[1]Department of Physics, University of Toronto, Toronto, ON, Canada
[2]School of Earth and Environment, University of Leeds, Leeds, UK
[3]National Centre for Earth Observation, University of Leeds, Leeds, UK
[4]Department of Physics and Atmospheric Science, Dalhousie University, Halifax, NS, Canada
[5]National Centre for Atmospheric Science, University of Leeds, Leeds, UK
[6]Air Quality Research Division, Environment and Climate Change Canada, Toronto, ON, Canada
[7]LATMOS/IPSL, UVSQ Université Paris-Saclay, Sorbonne Université, CNRS, Guyancourt, France
[8]NorthWest Research Associates, Socorro, NM, USA
[9]Department of Physics, New Mexico Institute of Mining and Technology, Socorro, NM, USA
[10]Jet Propulsion Laboratory, California Institute of Technology, Pasadena, CA, USA

Key Points:

- Record low ozone columns (<200 DU) were observed over Eureka in spring 2020
- Limited dynamical resupply of ozone and chemical destruction both contributed to reduced ozone columns
- Mean chemical ozone loss of 111-127 DU (27-31%) represents similar absolute loss and greater relative loss compared to that in spring 2011

Corresponding author: K. Bognar, kbognar@atmosp.physics.utoronto.ca

Corresponding author: K. Strong, strong@atmosp.physics.utoronto.ca

Abstract

In the winter and spring of 2019/2020, the unusually cold, strong, and stable polar vortex created favorable conditions for ozone depletion in the Arctic. Chemical ozone loss started earlier than in any previous year in the satellite era, and continued until the end of March, resulting in the unprecedented reduction of the ozone column. The vortex was located above the Polar Environment Atmospheric Research Laboratory in Eureka, Canada (80 °N, 86 °W) from late February to the end of April, presenting an excellent opportunity to examine ozone loss from a single ground station. Measurements from a suite of instruments show that total column ozone in 2020 was at an all-time low in the 20-year dataset, 22 to 102 DU below previous records set in 2011. Ozone minima (<200 DU), enhanced OClO and BrO slant columns, and unusually low HCl, $ClONO_2$, and HNO_3 columns were observed in March. Polar stratospheric clouds were present as late as 20 March, and ozonesondes show unprecedented depletion in the March and April ozone profiles (to <0.2 ppmv). While both chemical and dynamical factors lead to reduced ozone when the vortex is cold, the contribution of chemical depletion was exceptional in spring 2020 when compared to typical Arctic winters. The mean chemical ozone loss over Eureka was estimated to be 111-127 DU (27-31%) using April measurements and passive ozone from the SLIMCAT chemical transport model. While absolute ozone loss was generally smaller in 2020 than in 2011, percentage ozone loss was greater in 2020.

Plain Language Summary

While an ozone hole forms over Antarctica every year, the Arctic typically doesn't experience such dramatic ozone loss. The chlorine and bromine (halogen) reactions that destroy ozone require very low temperatures that are rarely observed in the Arctic stratosphere. The winter and spring of 2019/2020, however, was unusually cold in the Arctic, and consequently, a large amount of ozone was destroyed by halogen chemistry. To understand the behaviour of ozone in spring 2020, we use measurements from the Polar Environment Atmospheric Research Laboratory in Eureka, Canada. Eureka (at 80 °N) is one of the northernmost research stations in the world, and thus an ideal location to observe ozone loss. Spring 2020 ozone minima were lower than any in the 20-year dataset, and ozone destruction was ongoing until the end of March, which is rare in the Arctic. While ozone concentrations are largely determined by circulation patterns in the Arctic stratosphere, chemistry in spring 2020 was a much larger factor than usual. Halogen chemistry destroyed 27-31% of the total ozone, compared to about 10% in a typical winter. The only year on record with comparable ozone loss is 2011, and a larger percentage of the ozone column was lost in 2020.

1 Introduction

During the spring of 2020, ozone loss in the Arctic stratosphere reached levels previously observed only in spring 2011 (Manney et al., 2020). Ozone loss was near complete at some altitudes, reminiscent of the Antarctic ozone hole (Wohltmann et al., 2020). Ozone depletion in the Arctic is typically less severe and more variable than in the Antarctic stratosphere, due to the large interannual variability of the Arctic polar vortex (e.g., WMO, 2018). The Arctic vortex is generally warmer, weaker, and more irregular, largely because of greater wave activity than in the Antarctic stratosphere. Combined with the significant impact of stratospheric dynamics on ozone variability (e.g., Tegtmeier et al., 2008), these conditions often generate a springtime column ozone maximum in the Arctic.

In order for significant chemical ozone loss to take place in the Arctic, the vortex needs to be strong and stable (undisturbed) throughout the winter and spring. The strong circulation isolates the airmass inside the vortex, and during the winter, temperatures can drop below the (pressure-dependent) thresholds for polar stratospheric cloud (PSC)

formation. HNO_3 might be incorporated into supercooled ternary solution (STS) droplets or frozen nitric acid trihydrate (NAT) particles below ∼195 K in the lower stratosphere (Type I PSCs). Water ice particles form below ∼188 K (Type II PSCs) (e.g., WMO, 2014). PSCs (and other cold aerosols) then provide surfaces for the heterogeneous release of active chlorine from its reservoir species, HCl and $ClONO_2$ (Solomon et al., 1986). PSCs might also grow large enough to sediment, removing HNO_3 (a reservoir for NO_2) from the stratosphere. This leads to the denitrification of the vortex, and hinders chlorine deactivation via NO_2 (Salawitch et al., 1989; WMO, 2014). With the return of sunlight in the spring, active chlorine is rapidly photolyzed, and ozone depletion proceeds through the self-reaction of ClO (Molina & Molina, 1987) and the cross-reaction of ClO with BrO (McElroy et al., 1986; Tung et al., 1986). In the absence of NO_2 to deactivate chlorine, ozone loss can continue as long as the vortex remains cold and continues to act as a transport barrier. The Arctic vortex, however, is often weak or already broken down by early March (e.g., Manney, Santee, et al., 2011; Lawrence et al., 2018, and references therein), preventing large-scale ozone depletion. For significant ozone loss to occur, the interplay of several factors is required, such that the vortex becomes strong, cold, and long-lasting.

The winter of 2019/2020 stands as the best example of such conditions to date (e.g., Manney et al., 2020; Lawrence et al., 2020). While the size of the vortex was close to the average for much of the winter, it maintained a more or less constant size to become one of the largest by April. Potential vorticity (PV) gradients, a qualitative measure of the vortex stability in the lower stratosphere, set all-time records from February to April, indicating that the vortex acted as an exceptionally strong barrier to mixing and transport (Lawrence et al., 2020). Temperatures inside the vortex remained below the threshold for Type I PSCs (T_{NAT}) from early December to late March (the longest on record). As a result, chlorine activation was apparent by late November, 2019, with high ClO concentrations persisting until the end of March (Manney et al., 2020). Lawrence et al. (2020) argued that given the exceptional conditions outlined above, the winter of 2019/2020 had the greatest ozone loss potential ever observed. While various methods of estimating ozone loss have large uncertainties (e.g., Griffin et al., 2019; Manney et al., 2020), and dynamical contributions to low ozone columns need to be considered (Tegtmeier et al., 2008), measurements suggest that spring 2020 set new records for ozone depletion in the Arctic. Minimum lower stratospheric ozone concentrations observed from satellites (Manney et al., 2020) and ozonesondes (Wohltmann et al., 2020) were far smaller than previously seen, approaching levels typical for the Antarctic ozone hole. Ozone columns were anomalously low across the Arctic (Bernhard et al., 2020; Grooß & Müller, 2020; Inness et al., 2020; Lawrence et al., 2020).

The previous winter with the most significant ozone loss was 2010/2011 (Balis et al., 2011; Manney, Santee, et al., 2011; Sinnhuber et al., 2011; Adams, Strong, Zhao, et al., 2012; Kuttippurath et al., 2012; Lindenmaier et al., 2012; Pommereau et al., 2013; Strahan et al., 2013; Hommel et al., 2014; Solomon et al., 2014). The two seasons were similar in many respects, with a persistent, strong, and cold vortex (Lawrence et al., 2020). Ozone depletion, however, started later in 2010/2011 than in 2019/2020 (Manney et al., 2020). In addition, the minimum ozone values in 2011 did not drop as low as in 2020, and the minima occurred at higher altitudes. As a result, the total ozone column was affected less in 2011 than in 2020 (Manney et al., 2020; Wohltmann et al., 2020). Estimates of vortex-averaged chemical loss in the ozone column for 2011 vary based on the methods, satellite instruments, and altitude ranges used, with reported values ranging from 84-130 DU in the lower stratosphere (Sinnhuber et al., 2011; Kuttippurath et al., 2012; Strahan et al., 2013) and 120-170 DU for the total column (Manney, Santee, et al., 2011; Pommereau et al., 2013).

Significant Arctic ozone loss was also observed in the springs of 1996, 2000, and 2005 (Rex et al., 2004; Manney et al., 2006; Rex et al., 2006; Tilmes et al., 2006; Feng et al., 2007). The vortex during these winters was particularly cold, but ozone depletion ceased

much earlier than in 2011 (Manney, Santee, et al., 2011) or 2020. The duration of the cold period is key for large-scale ozone depletion, and the only year other than 2011 and 2020 with a large portion of the vortex below T_{NAT} going into March was 1997 (Coy et al., 1997; Manney et al., 1997; Newman et al., 1997). The polar vortex in 1997 (along with the vortex in 2020) was the largest on record for the March to early May period. Temperatures below T_{NAT} persisted until late March, but the volume of cold air was very limited until mid-January. This effectively delayed the depletion season by over a month compared to 2019/2020. As a result, ozone loss in 1997 was less than in any of the aforementioned years (Manney, Santee, et al., 2011). The 2015/2016 season started with record-breaking low temperatures, the formation of ice PSCs, and significant dehydration of the vortex. An early final warming, however, broke up the vortex by early March, preventing ozone loss on the scale of 2011 or 2020 (Manney & Lawrence, 2016; Matthias et al., 2016; Johansson et al., 2019).

Given the large interannual variability of the polar vortex, long-term measurements are necessary to assess stratospheric ozone depletion. Measurement stations in the Arctic provide valuable data, but only when the vortex position is favorable. Here, we report measurements from the Polar Environment Atmospheric Research Laboratory (PEARL) (Fogal et al., 2013) in Eureka, Canada (80 °N, 86 °W). Measurements inside the spring 2011 vortex have been used in several studies to assess ozone depletion (Adams, Strong, Zhao, et al., 2012; Lindenmaier et al., 2012; Adams et al., 2013; Pommereau et al., 2013), and in 2020, the vortex was located above Eureka longer than in any previous year in the measurement record. The datasets used here include long-term measurements of springtime trace gas columns from zenith-scattered-light differential optical absorption spectroscopy (ZSL-DOAS) instruments, a Fourier transform infrared (FTIR) spectrometer, a Brewer spectrophotometer, and a Pandora spectrometer. In addition, we use measurements from a Rayleigh-Mie-Raman lidar to identify PSCs, and simulations from the SLIMCAT chemical transport model to quantify chemical ozone loss.

This paper aims to assess the unprecedented spring 2020 ozone depletion in the context of the 20-year time series from PEARL, with an emphasis on the similarities and differences between 2020 and 2011. The paper is organized as follows: the datasets are described in Section 2. The time series of ozone and other trace gases are discussed in Section 3.1. Dynamical contributions to low ozone columns are examined in Section 3.2, and estimates of chemical ozone loss are discussed in Section 3.3. Our conclusions are given in Section 4.

2 Datasets and Methods

The DOAS and FTIR instruments used in this study are located in the PEARL Ridge Lab (610 m asl). The Ridge Lab (known as the Arctic Stratospheric Ozone Observatory prior to 2005) is one of the three facilities that make up PEARL, and is operated by the Canadian Network for the Detection of Atmospheric Change (CANDAC). The Ridge Lab is located 15 km from the Environment and Climate Change Canada (ECCC) Eureka Weather Station (EWS), while the other two PEARL facilities are within or near EWS. PEARL is part of the Network for the Detection of Atmospheric Composition Change (NDACC), and the ZSL-DOAS and Bruker FTIR instruments follow standards and best practices outlined by the relevant NDACC working groups.

Springtime measurements at PEARL are supported by the Canadian Arctic ACE/OSIRIS Validation Campaigns (Kerzenmacher et al., 2005), organized yearly since 2004. For the purposes of this paper, we use data from the first measurement date to 5 May in each year. Any yearly or overall averages refer to this period, unless specified otherwise. The measurement periods, data products, and mean uncertainties for each instrument are shown in Table 1, and the details are given in the following sections.

Table 1. Trace gas measurements used in this study, with mean relative uncertainties for each data product. Measurements up to 5 May in each year are included in the averages. The ozone and NO_2 products from the DOAS instruments (GBS, SAOZ) are 0-60 km total columns and 12-60 km partial columns, respectively The BrO and OClO products are dSCDs. Data products from the Bruker FTIR, Brewer and Pandora instruments are direct-sun total columns.

Instrument	Availability	Data products and mean uncertainty (%)						
		O_3	NO_2	BrO	OClO	HCl	$ClONO_2$	HNO_3
GBS	1999–2020	6.3	20.2	26.0[a]	24.2[a]	–	–	–
SAOZ	2005–2020	5.9[b]	13.9[b]	–	–	–	–	–
Bruker FTIR	2007–2020	5.4	8.4	–	–	2.1	12.0	19.7
Brewer #69	2001–2020	0.5[c]	–	–	–	–	–	–
Pandora	2019–2020	0.4[c]	–	–	–	–	–	–

[a]UV dSCDs (2007–2020), only including data over the detection limit
[b]Estimates, see text
[c]Random uncertainty only, see text

2.1 ZSL-DOAS Measurements

The GBS (Ground-Based Spectrometer) dataset (ozone and NO_2) is comprised of measurements from two instruments, the University of Toronto GBS (UT-GBS) and the PEARL-GBS (Fraser et al., 2009). Both instruments are ultraviolet-visible (UV-vis) triple-grating spectrometers, with cooled charge-coupled device (CCD) detectors and a ∼1° field-of-view. Springtime UT-GBS measurements are available for 1999-2020 (except for 2001 and 2002), and springtime PEARL-GBS measurements are available for 2007-2020. Since the two instruments are very similar and their measurements show excellent agreement, the datasets have been merged to create a single GBS dataset (Bognar et al., 2019). The SAOZ (Système d'Analyse par Observation Zénithale) instruments are part of a global network of similar instruments (Pommereau & Goutail, 1988). SAOZ instruments are UV-vis spectrometers with a fixed grating, an uncooled 1024-pixel linear photodiode array detector, and a ∼20° field-of-view. The dataset is constructed from measurements of two identical instruments, SAOZ-15 (2005-2009) and SAOZ-7 (2010-2020) (Bognar et al., 2019).

The instruments utilize the DOAS technique (Platt & Stutz, 2008) to retrieve stratospheric trace gas concentrations. Differential slant column densities (dSCDs) of ozone were retrieved in the 450-550 nm wavelength range for both instruments. The NO_2 dSCDs were retrieved in the 425-490 nm range for the GBS dataset, while the SAOZ retrieval used 410-530 nm. The DOAS analysis for the GBS and SAOZ datasets differs in the use of daily and yearly reference spectra, respectively. The dSCDs were converted to vertical column densities using the retrieval settings recommended by the NDACC UV-vis Working Group (`http://ndacc-uvvis-wg.aeronomie.be/`, see also Hendrick et al., 2011). The ZSL-DOAS ozone columns represent ozone from the surface to 60 km (referred to as total columns), while ZSL-DOAS NO_2 columns are 12-60 km partial columns, as determined by the standard NDACC air mass factor look-up tables used in the retrievals. For a more detailed description of the ZSL-DOAS instruments and retrieval procedures, as well as comparisons of the GBS and SAOZ data, see Bognar et al. (2019).

In addition to ozone and NO_2 measurements in the visible range, the GBS instruments also measure in the UV. OClO and BrO dSCDs were retrieved in the 350-380 nm and 345-359 nm ranges (Adams, Strong, Zhao, et al., 2012; Zhao, Strong, et al., 2016, respectively), using spectra averaged in 0.5° solar zenith angle (SZA) bins. The dSCDs were then averaged between 89° and 91° SZA. Based on the mean DOAS fitting error

and the standard deviation of dSCDs in the 89-91° SZA range, the 3σ detection limits were estimated to be 4.87 $\times 10^{13}$ molec cm^{-2} for OClO and 1.10 $\times 10^{14}$ molec cm^{-2} for BrO. OClO and BrO dSCDs are only reported when 90° SZA is available (until mid-April).

Uncertainty calculations for the ZSL-DOAS instruments are described in Bognar et al. (2019). The mean uncertainties for the measurement period (Table 1) are 6.3%, 20.2%, 24.2%, and 26.0% for the GBS ozone total columns, NO_2 partial columns, and OClO and BrO dSCDs, respectively. The SAOZ uncertainties only include the DOAS fitting error. The total uncertainty of SAOZ ozone data was estimated to be 5.9% by Hendrick et al. (2011). SAOZ NO_2 measurements have an estimated precision of 1.5 $\times 10^{14}$ molec cm^{-2} and accuracy of 10%. Combined in quadrature, this yields a total uncertainty of 13.9% for the SAOZ NO_2 measurements used here.

2.2 Direct-Sun Measurements

The CANDAC Bruker IFS 125HR Fourier transform infrared spectrometer (Bruker FTIR, Batchelor et al., 2009) measures solar absorption spectra using liquid-nitrogen cooled detectors (either a mercury cadmium telluride or an indium antimonide detector) and a potassium bromide beamsplitter. The measurements cover 600-4300 cm^{-1} with a resolution of 0.0035 cm^{-1}. No apodization is applied to the measurements. Springtime Bruker FTIR measurements are available for 2007-2020.

The Bruker FTIR uses the SFIT4 version 0.9.4.4 retrieval algorithm (based upon the methods of Pougatchev et al., 1996) with the HITRAN 2008 spectroscopic line lists (Rothman et al., 2009) to retrieve volume mixing ratios of trace gases. SFIT4 uses optimal estimation to iteratively adjust the retrieved profiles to best fit the measured solar-absorption spectra (Rodgers, 2000). The ozone, HCl, $ClONO_2$, and HNO_3 retrievals use the settings recommended by the NDACC Infrared Working Group (`https://www2.acom.ucar.edu/irwg`), while NO_2 is currently not a standard NDACC product. The NO_2 retrieval settings are described in Bognar et al. (2019). For all of the retrievals, the a priori profiles are provided by 40-year average (1980-2020) profiles from the Whole Atmosphere Community Climate Model (WACCMv4, Eyring et al., 2007; Marsh et al., 2013), while daily pressure and temperature profiles used in the retrievals are provided by the U.S. National Centers for Environmental Prediction (NCEP). The retrievals are performed on a 47-layer grid (0.61 to 120 km), and only the integrated total columns are used here.

A full error analysis for all species was performed following Rodgers (2000). The uncertainties include smoothing error, forward model parameter error, and measurement noise error. Adding these in quadrature, the mean uncertainties for the retrieved total columns of ozone, NO_2, HCl, $ClONO_2$, and HNO_3 are 5.4%, 8.4%, 2.1%, 12.0%, and 19.7%, respectively (Table 1). For a detailed description of the error budget calculations, see Batchelor et al. (2009). The averaging kernels indicate that for each trace gas, the retrievals have good sensitivity to the lower stratosphere (Batchelor et al., 2009; Lindenmaier et al., 2012), with mean degrees of freedom for signal (DOFS) of 3.3, 1.3, 2.7, 1.1, and 2.7 for ozone, NO_2, HCl, $ClONO_2$, and HNO_3, respectively. Results for all species were filtered using an RMS:DOFS filter, and retrievals with negative volume mixing ratios (VMRs) were rejected. One exception is HCl, where negative VMRs were accepted in order to increase the number of valid measurements in low-HCl conditions (2011 and 2020). Negative VMRs rarely occur in retrievals for the other species.

Brewer spectrophotometers measure the intensity of direct sunlight in narrow wavelength bands in the UV range using a holographic grating (Kerr, 2002). Ozone total columns are calculated from relative intensities at 310.1, 313.5, 316.8, and 320 nm. The Brewer instruments have been designated as the Wold Meteorological Organization Global Atmosphere Watch standard ozone monitoring instrument since the 1980s, and more than 230 Brewers have been deployed to date (Zhao et al., 2020). While multiple Brewers are located in Eureka, only data from Brewer #69 is used here, since that instrument has

the longest dataset of all the Brewers that have measurements for 2020. Brewer #69 is a MKV single monochromator that took measurements from 2001 to 2020 from the roof of the EWS building. Ozone columns are calculated from an average of five successive measurements. To avoid straylight, which affects single Brewers at high SZA, data with air mass factors greater than 5 (SZA>79.5°) and standard deviations greater than 2.5 DU were excluded. The random uncertainty of Brewer measurements was estimated to be 0.5% by Zhao et al. (2020), and the mean of the reported standard deviations in the filtered Brewer #69 dataset is 0.3%.

A Pandora spectrometer (#144) has been deployed at the PEARL Ridge Lab since February 2019. This instrument is the first Pandora spectrometer deployed in the polar regions (`https://www.pandonia-global-network.org/`). The Pandora instruments use a temperature-stabilized grating spectrometer and a CCD detector (Herman et al., 2009; Tzortziou et al., 2012). While Pandora #144 utilizes a combination of viewing geometries (including direct-sun, direct-moon, zenith-sky, and multi-axis), only the direct-sun ozone measurements are used here. Other Pandora measurements at Eureka will be a subject of a separate study. The direct-sun spectra are analyzed using the total optical absorption spectroscopy (TOAS) technique (Cede, 2019), and ozone is retrieved in the 310-330 nm range. The Pandora standard ozone column data products have a temperature dependence (Herman et al., 2015; Zhao, Fioletov, et al., 2016). This temperature dependence introduces a 1 to 3% seasonal bias between the Pandora and the Brewer standard data products (Zhao et al., 2020). Thus, the Pandora ozone data are corrected by an empirical method with the ozone-weighted effective temperature (Zhao, Fioletov, et al., 2016). The random uncertainty of Pandora ozone measurements was estimated to be 0.4% by Zhao, Fioletov, et al. (2016).

2.3 Additional Data Sets

The CANDAC Rayleigh-Mie-Raman Lidar (CRL) is a ground-based zenith-pointing lidar located at the Zero-altitude PEARL auxiliary laboratory (0PAL) at Eureka. The CRL transmits 532 nm and 355 nm light generated by separate, but co-aligned, Nd:YAG lasers. A 1 m telescope and eight photomultiplier tubes capture backscattered light at seven wavelengths: Rayleigh elastic channels at 532 nm, 532 nm with depolarization, and 355 nm; Raman channels for molecular nitrogen at 387 and 607 nm and for water vapour at 408 nm; and Rotational Raman channels at 528 and 531 nm. A complete description of the original configuration of the CRL is available in Nott et al. (2012), and an updated description of the depolarization system is given in McCullough et al. (2017). The CRL focuses on tropospheric cloud and aerosol measurements at high temporal and vertical resolution (1 minute × 7.5 metre; see McCullough et al., 2019). Binning the data (e.g. 30 minute × 150 m) allows the CRL to also provide data products well into the stratosphere. The two elastic backscatter channels (532 nm and 355 nm) can be used to detect PSCs.

Ozonesondes are launched on a weekly basis from EWS (Tarasick et al., 2016). During the intensive phase of the Canadian Arctic ACE/OSIRIS Validation Campaigns (2004-2020, typically early March), ozonesondes are launched daily, weather permitting. In addition to providing information for the estimation of ozone loss, ozonesondes were used in the GBS retrievals (Bognar et al., 2019), and to initialize the photochemical box model used for NO_2 diurnal scaling (Sect. 3.1). Radiosondes are launched twice daily, weather permitting, from EWS. Radiosonde temperature profiles were used to verify that candidate PSC cases identified by CRL (Sect. 3.1) were found within temperature regimes consistent with PSC formation: regions above the first tropopause, and with temperature less than the threshold temperature for Type I PSC formation (T_{NAT}). The first tropopause was identified as the lowest altitude at which the lapse rate was less than 2 K km^{-1}, and for which the average lapse rate over the following 2 km also did not exceed 2 K km^{-1} (WMO, 1957).

To select measurements inside the polar vortex, we used derived meteorological products (DMPs) (Manney et al., 2007) from the second Modern-Era Retrospective analysis for Research and Applications (MERRA-2). MERRA-2 is an atmospheric reanalysis that utilizes the Goddard Earth Observing System Model Version 5.12.4 reanalysis system (GEOS-5) (GMAO, 2015; Gelaro et al., 2017). Values of scaled potential vorticity (sPV) (Dunkerton & Delisi, 1986; Manney et al., 1994) and temperature were calculated along the line-of sight of the ground-based instruments (for each individual measurement time), and vertically for SLIMCAT columns and radiosondes, using the Jet and Tropopause Products for Analysis and Characterization (JETPAC) package (Manney, Hegglin, et al., 2011). The line-of-sight calculations for the ZSL-DOAS instruments are described in Adams, Strong, Batchelor, et al. (2012). It should be noted that unlike for direct-sun measurements, exact line-of-sight calculations are not possible for the ZSL-DOAS instruments, due to the multiple paths taken by scattered sunlight before reaching the detectors. The approximate nature of the ZSL-DOAS DMPs, combined with the long integration times corresponding to each vertical column (2-4 hours, 30-60° change in the solar azimuth), means the ZSL-DOAS results should be interpreted with caution when the vortex edge is near Eureka.

For the purposes of this study, the inner edge of the vortex was defined as sPV = 1.6×10^{-4} s^{-1}, and the outer edge as sPV = 1.2×10^{-4} s^{-1} (Manney et al., 2007). To filter out measurement that potentially sample through the vortex edge, sPV criteria were tested at 16, 18, and 20 km (the altitude range of maximum ozone concentrations) along the line-of-sight of each instrument. Measurements were considered to be inside (outside) the vortex if the sPV at all three altitudes was greater (less) than the inner (outer) vortex edge threshold. Measurements not matching these criteria were assumed to be on the vortex edge and were excluded from the analysis in this paper.

To investigate ozone loss inside the vortex, we use output from the TOMCAT/SLIMCAT (hereafter SLIMCAT) three-dimensional offline chemical transport model (Chipperfield, 2006; Dhomse et al., 2013; Chipperfield et al., 2015; Dhomse et al., 2019). The model is forced by ERA5 analyses provided by the European Centre for Medium-Range Weather Forecasts (Hersbach et al., 2020), and the chemistry component is performed separately for each time-step. SLIMCAT includes both active ozone, for which the full chemistry and dynamics are considered, and passive ozone, which is dynamical tracer with no chemistry. Passive ozone is set equal to active ozone on 1 December of each year. Passive ozone can be used to estimate chemical ozone loss as the difference between passive and active (or measured) ozone (e.g., Feng et al., 2007; Singleton et al., 2005, 2007; Adams, Strong, Zhao, et al., 2012; Lindenmaier et al., 2012; Dhomse et al., 2013). Here we use 6-hourly model output for 2000-2020, interpolated to the geolocation of Eureka. Column values were calculated from trace gas VMR profiles using modeled pressure and temperature profiles.

3 Results and Discussion

3.1 The Spring 2020 Measurements in Context

The polar vortex was located above or near Eureka for much of spring 2020. All instruments sampled continuously inside the vortex from 25 February through 31 March. Before that, the earliest SAOZ measurements (20-22 February) were inside the vortex, and the ZSL-DOAS instruments sampled through the vortex edge on 23-24 February. In April and May, the vortex location was more variable. The instruments measured inside the vortex for 9-18 and 27-30 April, mostly through the vortex edge for 1-7 and 19-26 April, and on the edge or outside the vortex from 1 May on. The exceptional longevity of the vortex (Lawrence et al., 2020) is evidenced by the fact that 30 April is the latest in-vortex measurement (by two weeks) in the 20-year dataset presented here. It should be noted that the number of in-vortex measurements depends on the location of the vor-

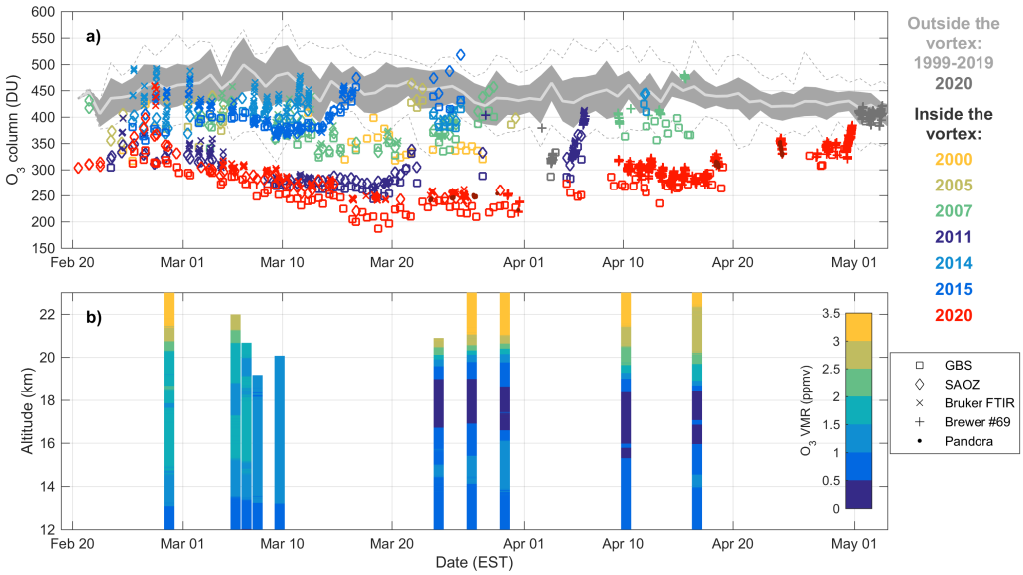

Figure 1. **a)** Measurements of total column ozone (DU) from the GBS, SAOZ, Bruker FTIR, Brewer, and Pandora instruments. Measurements outside the vortex in the time series of all instruments (up to 2019) are represented by the gray shaded area (daily mean and standard deviation) and the gray dashed lines (daily minima and maxima). The colored datapoints represent measurements inside the vortex, in years when the vortex was located above Eureka for a substantial part of the measurement period. In addition, 2020 measurements outside the vortex are plotted separately in dark gray. **b)** Ozone mixing ratio profiles (ppmv) from 2020 ozonesonde measurements. Only sondes that reached altitudes above 18 km are shown.

tex, and also on the measurement coverage of the individual instruments. Direct-sun measurements require clear conditions, and unfavorable weather can significantly reduce measurement coverage, especially for the early spring (high SZA). ZSL-DOAS instruments, on the other hand, measure in cloudy conditions as well, but provide data for twilights only. Measurements in 2020 faced additional challenges as a result of the COVID-19 pandemic. The Bruker FTIR and SAOZ measurements ended on 26 and 30 March, respectively, due to lack of on-site support. GBS measurements, however, continued for the rest of the spring, and Brewer #69 measurements (which typically start in late March) provided direct-sun data for the rest of the spring. Pandora direct-sun measurements are limited to a few days in spring 2020, due in part to the lack of on-site support.

Figure 1a shows measurements of ozone columns inside and outside the vortex for the full time series of all instruments. The 2020 measurements are exceptional, both considering the duration of in-vortex measurements, and the record low ozone columns. Ozone values inside the vortex show a clear decline through March, and all instruments recorded the all-time lowest values in their respective time series in the second half of March 2020. The GBS time series has the best coverage in spring 2020, and the lowest ozone values appear in this dataset, with ozone columns near or below 200 DU (minimum of 187 DU) for 16-19 March. SAOZ measurements show a minimum (221 DU) on March 16, although SAOZ has no measurements for 17-19 March. Bruker FTIR ozone columns were in the 240-250 DU range for 16-19 March, while the minimum value (240 DU) was reached on 26 March. The GBS and SAOZ instruments also measured column values between 210 and 250 DU in late March. The Brewer and Pandora datasets start on 30 and 23 March,

respectively, and the minimum values (218 DU and 222 DU, respectively) were measured on 31 March for both instruments. The scatter between the various instruments is expected, and the GBSs generally measure the least ozone among the various instruments (Adams, Strong, Batchelor, et al., 2012; Bognar et al., 2019). The GBS and Brewer time series continue (with good coverage) through April and early May, and show the gradual increase of ozone inside the vortex. The vortex was still strong (and ozone columns inside were still below background levels) by the end of April.

The decline of ozone columns inside the vortex in early March was similar to that in 2011, the only previous year with comparable ozone columns in the dataset. Minimum values in 2020, however, were much lower than those observed in 2011. GBS, SAOZ, and Bruker FTIR measurements all reached their minima on 18 March 2011. In 2020, minimum ozone columns measured by the same instruments were lower by 56, 43, and 22 DU, respectively. Minimum ozone in the Brewer dataset was 102 DU lower in 2020 than in 2011, although Brewer #69 generally has few measurements inside the vortex. While the vortex moved away from Eureka in late March of 2011, there is no indication that ozone columns reached minima similar to 2020. Other years when the vortex spent a significant amount of time above Eureka do not show ozone columns comparable to 2011 and 2020 (nearest minima are 93-143 DU higher than the lowest 2020 values). Ozone supply, however, is variable from year to year (e.g., Tegtmeier et al., 2008), and a cold stratosphere generally corresponds to reduced ozone columns even without chemical depletion. Part of the record low column ozone in 2020 is likely related to dynamics, and this is examined further in Section 3.2.

Figure 1b shows ozone profiles measured by ozonesondes in spring 2020. The gradual depletion of ozone in the 16-20 km altitude range is apparent by early March, and the same altitude range shows exceptionally low mixing ratios in late March and April. Mixing ratios were consistently below 0.5 ppmv in a wide altitude range (with minima below 0.2 ppmv), indicating near-complete depletion of ozone. Such low values are unprecedented in the Arctic: even in 2011, mixing ratios did not drop below 0.5 ppmv (e.g., Solomon et al., 2014). Ozonesonde profiles from other Arctic sites paint a consistent picture of ozone depletion that is unprecedented in the Arctic, and is more similar to Antarctic winters than any previously observed Arctic winter (Wohltmann et al., 2020). The altitude of the depleted layer likely explains some of the differences between the column measurements in Figure 1a. Estimated scattering heights for ZSL-DOAS instruments are below 16 km (Adams, Strong, Batchelor, et al., 2012). As a result, path lengths in the 16-20 km altitude range are several times longer for ZSL-DOAS instruments than for direct-sun measurements. The increased sensitivity to the region of depleted ozone likely contributes to the lower ozone columns measured by the ZSL-DOAS instruments.

Figure 2 shows complementary measurements from the GBSs and Bruker FTIR, along with temperatures from DMPs and radiosondes. BrO and OClO dSCDs retrieved from GBS measurements (Fig. 2a-b) were significantly above background levels in 2020. This indicates ongoing chlorine activation from the earliest measurements (5 March) to late March, with occasional enhancements in early April. BrO and OClO enhancements in 2011 were similar to 2020, although the 2011 time series is much shorter. There are no other years in the data record with persistent enhancements of both BrO and OClO. The highest BrO dSCDs were recorded in 2015, but these correspond to smaller OClO enhancements (and much higher ozone columns) than either 2011 or 2020.

Extremely low values of chlorine reservoirs HCl and $ClONO_2$ in the Bruker FTIR dataset (Fig. 2c-d) are consistent with the elevated OClO values in the GBS data, and indicate chlorine activation and heterogeneous chemistry on PSCs. HCl column values were consistently very low in March, with the exception of a few measurements in late February. $ClONO_2$ measurements follow the same pattern, with an additional minor peak mid-March. Both HCl and $ClONO_2$ show a gradual recovery from approx. 20 March to the end of the Bruker FTIR measurements (26 March). This increase corresponds to a

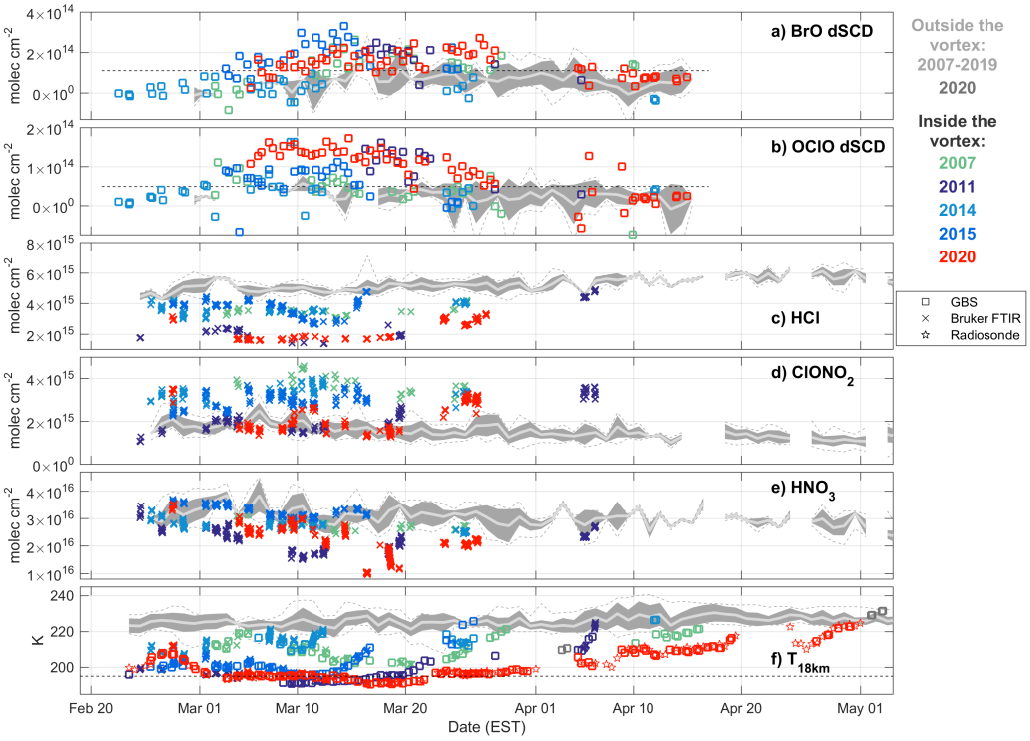

Figure 2. **a)** and **b)** Twilight measurements of BrO and OClO dSCDs from the GBS dataset. The approximate detection limits are indicated by the dashed lines. **c)** to **e)** Measurements of HCl, $ClONO_2$, and HNO_3 columns from the Bruker FTIR. **f)** Temperature at the 18 km level along the line of sight of the Bruker FTIR and GBS instruments, as well as T_{18km} from 2020 radiosonde measurements. The dashed line indicates T_{NAT} (195 K). Plot colors and shading as in Fig. 1a.

gradual decrease in the OClO dSCDs, consistent with conversion of active chlorine back into its reservoir species. These observations are generally consistent with satellite measurments of HCl and $ClONO_2$ presented by Manney et al. (2020). 2011 data tell a similar story, with low HCl and $ClONO_2$ column values into March, and a gradual recovery in late March. HCl values dropped slightly lower in 2011 than in 2020, whereas for $ClONO_2$, the all-time minima were measured in 2020. $ClONO_2$ recovery started later in 2020, likely due in part to the slow increase of NO_2 concentrations (Fig. 4). In the rest of the measurement record, HCl and $ClONO_2$ show a marked decrease only in 2015, consistent with moderate enhancements of OClO.

While low HCl and $ClONO_2$ columns point to the presence of PSCs, HNO_3 (the main component of Type I PSCs) was not exceptionally low in the early spring of 2020 (Fig. 2e). HNO_3 remained close to typical background values until the second half of March. On 16-19 March, however, HNO_3 columns dropped to the lowest values by far in the Bruker FTIR data record. Lower stratospheric temperatures from radiosondes and along the line-of-sights of the GBS and Bruker FTIR measurements (Fig. 2f) show that the same mid-March period saw the lowest temperatures in 2020. T_{18km} was well below T_{NAT}, creating prime conditions for PSC formation. $ClONO_2$ values reached their minimum in this cold period, but there was no discernible increase in the OClO dSCDs. Ozone columns also reached their minima on 16-19 March. CRL data indicate the presence of PSCs over

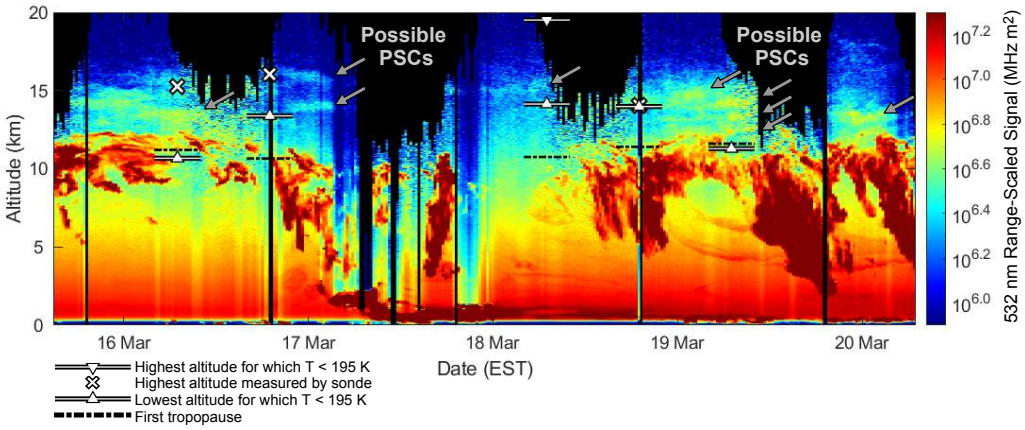

Figure 3. 532 nm range-scaled signal from the CRL for 16-20 March, during a period of PSC activity. Possible PSCs are particularly clear on 17 March as distinct features (∼0.5 km vertical extent) at 14 and 16 km, which are brighter than surrounding areas by a factor of approximately 2.5. Other regions showing possible PSCs are visible on 16-20 March, above 12 km. As per radiosonde temperature profiles, the PSC regions are all above the first tropopause (dot-dashed black lines; see text), and also have temperatures below T_{NAT} (195 K, lines with upward triangles). Black areas indicate low signal-to-noise ratios, generally due to the high solar background during daytime, and occasionally due to attenuation of the laser beam by tropospheric features below 12 km.

Eureka during 16-20 March. Figure 3 shows the 532 nm attenuated backscatter coefficient from the CRL for the 0-20 km altitude range. The features between 12 and 16 km that are narrow in their altitude extent are most likely PSCs. These are particularly visible on 17 March at 14 km and 16 km, again on 18 March at 15 km, and present on 16 and 18 March at 13 km through 16 km. These features return signals brighter than the surrounding molecular background by a factor of approximately 2.5. In early March, temperatures hovered near (but generally above) T_{NAT}, consistent with the higher HNO_3 values observed by the Bruker FTIR. Accordingly, there are no PSC candidates detected in March CRL data before 16 March. Coincident high OClO values and low HCl and $ClONO_2$ columns indicate that PSCs were likely present elsewhere in the vortex (as shown by DeLand et al., 2020, for example), and the discrepancies are likely explained by the different time-scales for vortex mixing (∼5-7 days) and chlorine deactivation (weeks) (e.g., Adams, Strong, Zhao, et al., 2012). It should be noted that the vertical distribution of HNO_3 was different in 2011 and 2020, and HNO_3 values were anomalously high before PSC formation started in 2019/2020 (Manney et al., 2020).

From mid-March into April, the 2020 vortex was the coldest among any year with measurements inside the vortex. Temperatures remained near T_{NAT} until the end of March, and only reached background values by the end of April. This slow warming correlates with the slow increase of ozone inside the vortex, as examined further in Section 3.2. While the vortex temperatures hovered around T_{NAT} for the entire month of March, the first observations in 2020 reveal higher temperatures in late February. This increase corresponds to peaks in the HCl, $ClONO_2$ and HNO_3 data. DMPs show that these measurements were taken near the vortex edge. The potential impact of mixing through the vortex edge manifests as an increase of the ozone and NO_2 columns (Figs. 1 and 4), as well as an increase in SLIMCAT passive ozone in the vortex (Sect. 3.3). Temperatures followed a different pattern in 2011. The lowest temperatures were observed around 10 March, T_{18km} increased gradually to early April, and then increased rapidly as the vortex moved

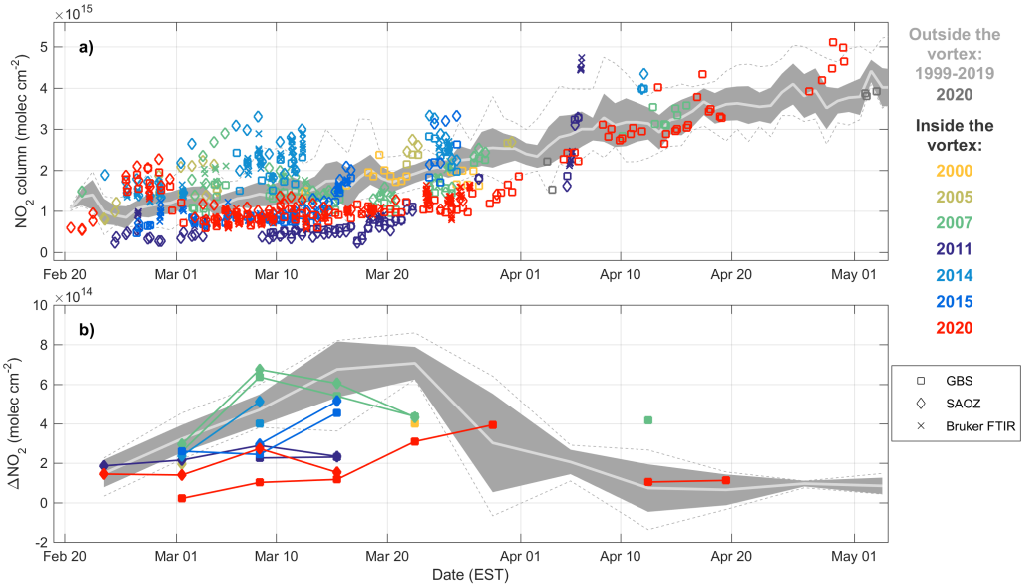

Figure 4. **a)** Measurements of NO_2 partial columns from the GBS and SAOZ instruments, and NO_2 total columns from the Bruker FTIR. The columns have been scaled to local noon. **b)** Weekly mean diurnal variability (evening minus morning) of NO_2 in the GBS and SAOZ measurements (without scaling). Mean values were calculated only if at least three daily values were available. Plot colors and shading as in Fig. 1a.

away from Eureka. Accordingly, HNO_3 measurements in mid-March were much lower in 2011 than in 2020. Chlorine reservoirs and OClO, on the other hand, show similar behaviour in both years, indicating the role of mixing in the vortex. Temperatures in 2015 were also quite low, hovering near T_{NAT} in March. The cold conditions did not last, however, and T_{18km} increased rapidly after 12 March.

NO_2 columns from the ZSL-DOAS instruments and the Bruker FTIR are shown in Figure 4a. To account for the diurnal variation of NO_2, partial columns were scaled to local noon using a photochemical box model (McLinden et al., 2000; Brohede et al., 2007). For more details on the scaling procedure, see Bognar et al. (2019) and Adams, Strong, Batchelor, et al. (2012). Aside from the peak in late February discussed above, NO_2 columns were generally low in 2020. Unlike other trace gases, NO_2 measurements did not reach record lows in early spring: in-vortex NO_2 in 2011 was consistently below 2020 values. The 2020 measurements are consistent with the higher HNO_3 column values measured by the Bruker FTIR (Fig. 2e). The mean diurnal increase of NO_2, on the other hand, was at its all-time minimum in both the GBS and SAOZ datasets in 2020 (Fig. 4b, no diurnal scaling). As a result, the usual seasonal recovery of NO_2 concentrations in the vortex proceeded much more slowly than in any other year in the measurement record, and NO_2 column values remained unseasonably low into late March. The diurnal increase of NO_2 only returned to background values in late March, coincident with the increase of $ClONO_2$ values (Fig. 2d). A minor (and temporary) NO_2 increase after 10 March corresponds to the $ClONO_2$ peak discussed earlier, and it is likely related to mixing and transport, as opposed to local chemistry. In 2011, NO_2 columns were consistently lower than in 2020, but the diurnal increase was slightly above 2020 values. NO_2 concentrations recovered rapidly during the 2011 vortex breakup (Adams et al., 2013), while the increase was more gradual in 2020. The only other year with con-

sistently low in-vortex NO_2 was 2015, but NO_2 values increased rapidly in mid-March, following similar trends in temperature and other trace gases. In other years, NO_2 in the vortex was generally above background levels.

In summary, all instruments used in this study measured record low ozone column values in spring 2020. The GBS, SAOZ, and Bruker FTIR instruments all measured the smallest (or close to the smallest) ozone columns (187-240 DU) in their respective time series on 16-19 March, well below 2011 minima. The same late March period also saw very low values of chlorine reservoirs HCl and $ClONO_2$, alongside temperatures below T_{NAT}, and an extraordinary drop in HNO_3 concentrations. These observations indicate the presence of PSCs (confirmed by CRL observations), and, combined with elevated OClO and BrO dSCDs, point to significant chemical ozone depletion. Ozonesonde profiles later in March (and well into April) showed unprecedented depletion of ozone in the 16-20 km altitude range, with mixing ratios below 0.2 ppmv. While the vortex was cold throughout the spring, T_{18km} was consistently above T_{NAT} in the early spring, and again past 21 March. HCl, $ClONO_2$, and NO_2 gradually recovered by late March, and OClO dSCDs decreased below the detection limit. This indicates that chemical ozone loss inside the vortex likely stopped by the end of March (perhaps slightly later than in 2011). The vortex above Eureka appeared less denitrified in 2020 than in 2011, consistent with higher HNO_3 columns in 2020. Ozone columns in 2020 remained well below seasonal averages until the end of April. Dynamical and chemical contributions to these record low ozone columns are discussed in the following sections.

3.2 The Impact of Dynamics

Accurate assessment of chemical ozone depletion in the Arctic is hindered by the fact that dynamical and chemical contributions to low ozone columns are difficult to separate. Approximately half of the variability in springtime ozone is due to interannual differences in ozone replenishment from above (Chipperfield & Jones, 1999; Tegtmeier et al., 2008). Since this replenishment is due to diabatic descent, resupply of ozone is generally smaller in cold winters, when diabatic descent is weaker. Mixing through the vortex edge also contributes to ozone variability, and less mixing in cold winters contributes to reduced ozone columns, especially in March (Salby & Callaghan, 2007). These factors (among others, see e.g., supplementary information of Manney, Santee, et al., 2011, and references therein) result in a good correlation between ozone and lower stratospheric temperature inside the vortex. On the other hand, since PSC formation is temperature-dependent, chemical ozone depletion also leads to a good correlation between ozone and temperature (e.g., Tilmes et al., 2006; Rex et al., 2006). The exact correlation, however, will depend on the balance of contributing factors, and so we might expect to see different relationships between ozone and temperature depending on the relative importance of chemistry and dynamics.

Figure 5 shows the relationship of in-vortex ozone columns and T_{18km} for the GBS, SAOZ, Bruker FTIR, and Brewer datasets. The black dots and black dashed lines show the correlation for what might be considered 'typical' springtime conditions. These years (including early measurements in 2011 and 2020) all experienced a similar balance of chemical depletion and dynamical factors. The R^2 values are similarly high for all datasets, and the slopes vary only slightly, in accordance with the differences between ozone columns from each instrument. Even the limited number of points for the Brewer follow this correlation. Measurements from 2015 follow a different correlation, indicated by the gray dots and gray dashed lines in Figure 5. The slopes are approximately parallel to the correlation for typical years discussed above, but with a significant positive offset. R^2 values are also high, but with more variability between the instruments. As shown in Figures 1a and 2f, 2015 was a relatively cold year with anomalously high ozone. The reasons for this are examined in detail by Manney et al. (2015). A minor warming in January 2015 caused unusually strong descent and high ozone values, with minimal chem-

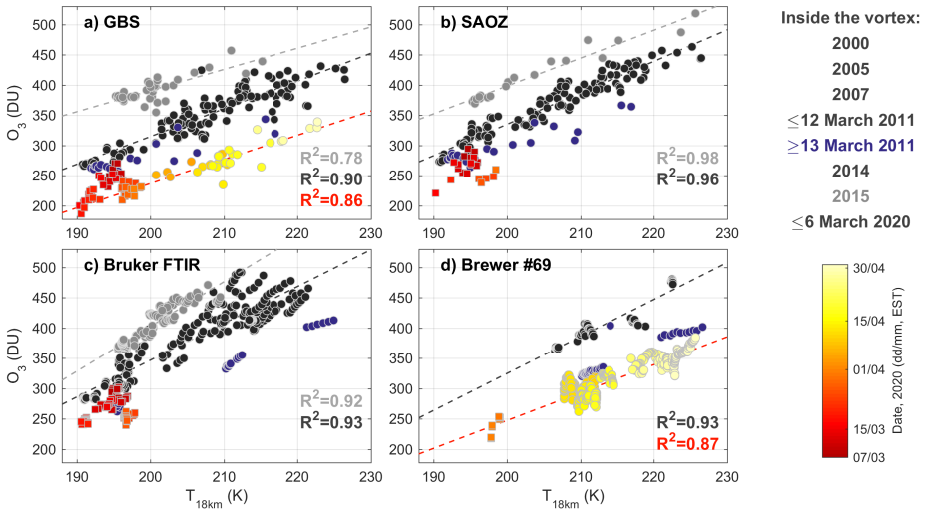

Figure 5. Ozone columns inside the vortex as a function of T_{18km} for **a)** the GBS, **b)** SAOZ, **c)** Bruker FTIR, and **d)** Brewer. In-vortex measurements for 'typical' years (alongside measurements from early spring 2011 and 2020) are shown in black, with a corresponding linear fit and R^2 value. In-vortex measurements for 2015 (and the corresponding linear fits and R^2 values) are plotted in gray. Measurements that start to deviate from the typical correlation (black dashed line) are plotted in blue for 2011, and with a color scale representing dates for 2020. For 2020, squares and dots correspond to March and April data, respectively. The red dashed lines show the linear fit for April 2020.

ical ozone destruction. It is then reasonable that the correlation of ozone and temperature would be different from typical years, since the contribution of chemical depletion was largely absent in 2015, tipping the balance towards the dynamical factors.

Measurements in spring 2020 are another special case. While measurements up to 6 March still keep to the correlation for typical years, data for the rest of March clearly follow a different trajectory. This is shown by the color scale squares in Figure 5. March ozone columns decrease more rapidly than expected for temperatures near and below T_{NAT}, and this behaviour is consistent across all instruments that have data in March. This indicates that chemistry was much more dominant than usual. Once chemical depletion stops in late March, ozone columns start increasing with temperature, but following a trajectory that is different from the correlation for typical years. The exceptionally long-lived vortex presents an opportunity to observe this recovery. The trajectory of ozone columns in April (color scale dots and red dashed lines in Fig. 5a, d) follows a line approximately parallel to the typical correlation, but with a significant negative offset. This offset (calculated at $T_{18km} = 210$ K) is 84 DU and 93 DU for the GBS and Brewer datasets, respectively, and might be interpreted as the approximate amount of additional chemical ozone destruction in 2020 compared to more typical Arctic winters. While adding late March data to the linear fits results in a very similar correlation, only April data were included, for consistency with the ozone loss estimates discussed in Section 3.3. 2011 measurements follow a trajectory similar to 2020 (see also Adams, Strong, Zhao, et al., 2012). Ozone columns start to clearly deviate from the typical correlation from 13 March onward. The few late-season measurements in 2011 correspond to the rapid increase of ozone on 4-6 April (Fig. 1a), and follow a trajectory with a negative ozone offset on the correlation plots. While direct comparisons are difficult given that the instruments mostly

measured outside the vortex after 23 March 2011, the ozone offset in Figure 5a and 5d is generally larger in 2020 than in 2011. These offsets highlight that chemical ozone destruction in both 2011 and 2020 was exceptional in the context of the data record presented here.

Measurements of HF from the Bruker FTIR can be used as another dynamical tracer. Since HF is long-lived and chemically unreactive, it can be used as a tracer of vertical motion (Mankin et al., 1990; Toon et al., 1992). HF columns increase when the air column is descending with replenishment at the top with air from neighbouring columns. As a result, HF columns are generally larger in the vortex than outside the vortex (Fig. S1a in the supporting information, hereafter "SI"). HF shows an increasing trend in the stratosphere (e.g. Griffin et al., 2017), and this trend has been accounted for before scaling with the HF columns (see SI). Inside the vortex, the smallest trend-corrected HF columns were measured in 2011, 2014, and 2020, and the largest columns were measured in 2015. This indicates unusually strong descent in 2015, consistent with Manney et al. (2015). To remove some of the dynamical effects from the Bruker FTIR dataset, we normalized the measurements of ozone, NO_2, HCl, $ClONO_2$, and HNO_3 with the HF columns (after Lindenmaier et al., 2012, but with trend-corrected HF columns). The results are shown in Figure S1b-f in the SI. Since column values of HF and other trace gases would change in unison if the main driver was dynamics, we assume that any decrease in the HF ratios is largely the result of chemistry. It should be noted that the trend correction changes the HF columns, but does not substantially impact the year-to-year variability of the HF ratios described below.

The 2020 time series of HF-normalized HCl and $ClONO_2$ show the same evolution as the columns in Figure 2c-d, with consistently low values in March, and a gradual increase past 20 March. The 2011 ratios are also similar to the column values, indicating that the extremely low columns of HCl and $ClONO_2$ in both years were primarily due to heterogeneous chemistry, and not variability of transport. The evolution of HF-normalized HNO_3 follows the same patterns as seen in Figure 2e, but the differences between individual years are smaller. The large drop in HNO_3 concentrations on 16-19 March 2020 is still apparent in the HF-normalized time series, confirming that HNO_3 was taken up on PSC particles. HF-Normalized NO_2 columns show that when accounting for dynamical differences, NO_2 levels were similarly low in 2020 and 2011. The slow increase of NO_2 columns in 2020 is apparent in the HF-normalized time series, in agreement with Figure 4b.

Compared to Figure 1a, the HF-normalized ozone time series tells a very similar story. HF-Normalized ozone was smaller in 2020 than in any previous year, with the minimum values recorded on 26 March (consistent with the Bruker FTIR ozone minima). Differences between 2020 and other years are reduced in the HF-normalized time series, as expected since transport generally plays a significant role in maintaining higher ozone concentrations inside the vortex. The trend-corrected HF columns indicate that vertical motion was likely similar in 2011 and 2020. The fact that HF-normalized ozone still reached all-time minima in 2020 further highlights the role of chemical ozone depletion. This is examined in more detail in the next section.

3.3 Estimates of Chemical Ozone Loss

The narrow altitude region of depleted ozone seen in the ozonesonde profiles (Fig. 1b), the sharp deviations from the typical relationship of ozone and temperature (Fig. 5), and record low HF-normalized ozone all indicate that chemical ozone loss played a large role in spring 2020. Since our instruments do not measure during the winter (polar night), we have no in-vortex measurements from periods with no chemical ozone depletion, and therefore cannot estimate ozone loss from the measurements alone. In order to quantify chemical ozone loss, we use the passive tracer method. Absolute ozone

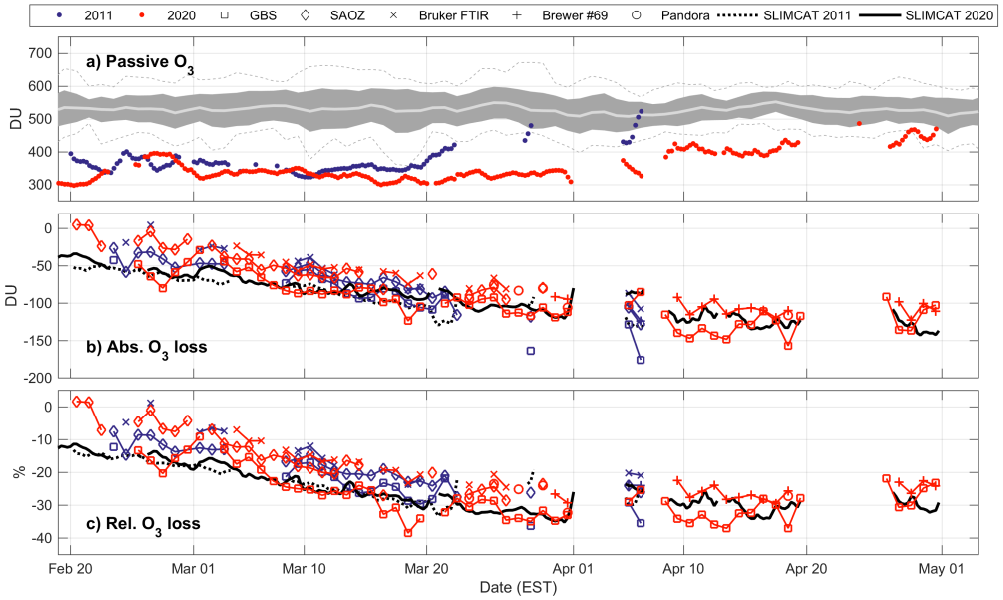

Figure 6. **a)** SLIMCAT passive ozone. The gray shaded area shows statistics of passive ozone (after Fig. 1) for years when the vortex was not present over Eureka. The colored points show in-vortex data for 2011 and 2020. **b)** Absolute and **c)** relative ozone loss inside the vortex for 2011 and 2020, calculated as described in the text. The datapoints show daily average loss for the measurements, and the black lines show 6-hourly values using SLIMCAT active ozone.

loss is calculated by subtracting measured ozone from SLIMCAT passive ozone, and relative ozone loss is calculated as absolute loss over passive ozone. It should be noted that empirical ozone loss estimates have large uncertainties, and passive subtraction could potentially overestimate ozone loss (Griffin et al., 2019, and references therein).

Comparisons between SLIMCAT results and measurements are included in the SI. SLIMCAT active ozone inside the vortex shows good agreement with all instruments (Fig. S2, S3), with mean relative differences (SLIMCAT minus measurements) of 1.4%, -3.9%, -8.9%, and -4.0% for the GBS, SAOZ, Bruker FTIR and Brewer data, respectively (in-vortex measurements for all years). The larger differences with respect to the Bruker FTIR dataset are partly due to spatial mismatch in late February (high-SZA measurements, see SI). HCl and $ClONO_2$ agree well with Bruker FTIR measurements inside the vortex (-4.0% and 0.6%, respectively), while HNO_3 columns show a negative bias (-18.1%). The underestimation of HNO_3 is likely related to the simple equilibrium denitrification scheme in the model (e.g., Feng et al., 2011). To assess SLIMCAT passive ozone, we used ozonesonde total columns from December of each year. The mean difference between passive ozone and the ozonesonde columns is 4.8±9.6 DU (2.0±2.7%, mean and standard error) for 2000-2018, indicating that SLIMCAT successfully simulates observed ozone before chemical depletion starts.

The passive ozone time series inside the vortex for 2020 is shown in Figure 6a. Passive ozone hovered around 300-350 DU for all of March, well below typical springtime values when the vortex is not present over Eureka (gray shading in Fig. 6a). This indicates that dynamical mechanisms, as discussed above, are in part responsible for the exceptionally low column values observed in the spring. Passive transport of ozone alone would have caused a year with ozone minima that were surpassed only by 2011, as in-

dicated by the very low values of out-of-vortex ozone measured in early April (gray points in Fig. 1a). Passive ozone in 2011 was as low as in 2020 until early March, but the two time series start to diverge after 10 March. Passive ozone in 2011 increased sharply in late March, and again in early April. These increases correspond well to the increases in the measured ozone columns (Fig. 1a).

Figure 6b-c show daily averages of absolute and relative ozone loss for all the instruments. SLIMCAT passive ozone was linearly interpolated to the measurement times, using only the datapoints that were inside the vortex based on vertical DMPs corresponding to the SLIMCAT ozone columns. Ozone loss values were taken to be inside the vortex only if both the measurement and the corresponding SLIMCAT column were inside the vortex. In 2020, chemical ozone loss was apparent by the end of February, and its magnitude gradually increased until the end of March. Loss estimates for individual instruments show some scatter, in accordance with the differences between ozone columns (Sect. 3.1). The GBS instruments measured the lowest ozone column values (Fig 1a), and therefore differences from passive ozone are most pronounced for this dataset. Absolute differences fell below 100 DU by mid-March, and reached 150 DU in April (maximum of 157 DU on 18 April). Relative differences show a similar pattern, with values well below 30% in the second half of March and in April. The maximum relative difference of 38% was reached on 18 March. SAOZ measurements are irregular past 14 March, and the last in-vortex measurement was on 29 March. The maximum difference of 95 DU (29%) occurred on the second to last measurement day, 26 March. Bruker FTIR measurement coverage is weather-dependent, and the in-vortex measurements ended on 26 March. The maximum difference of 81 DU (25%) was reached on that day. Brewer measurements started on 30 March, and consistently measured ozone more than 100 DU smaller than SLIMCAT passive ozone. The maximum absolute difference of 123 DU occurred on 28 April, while 29% relative difference was observed on both 31 March and 17 April. The Pandora instrument has only six days of in-vortex measurements. The maximum absolute and relative differences of 117 DU and 32% were observed on 18 April and 31 March, respectively.

Our loss estimates are generally similar for 2020 and 2011. Results using SLIMCAT active ozone (black lines in Fig. 6b, c) show that absolute loss was slightly higher in 2011. Relative loss was very similar, although ozone loss continued longer (to the end of March) in 2020, resulting in more overall relative loss. The measurements tell a similar story. The absolute differences generally overlap for 2011 and 2020, but the peak losses are greater for 2011. The daily peak loss from the GBS, SAOZ, Bruker FTIR and Brewer datasets was 176, 129, 108, and 124 DU, respectively, compared to 157, 95, 81, and 123 DU in 2020. Peak relative loss, on the other hand, was smaller in 2011 for all instruments, with values of 36, 28, 24, and 24%, compared to 38, 29, 25, and 29% in 2020. Overall, column ozone loss was similar between 2011 and 2020 despite the smaller VMRs reached in 2020 ozonesonde profiles (Manney et al., 2020; Wohltmann et al., 2020). This is largely explained by the higher passive ozone simulated by SLIMCAT for 2011 (Fig. 6a).

For the spring of 2011, previous studies report a range of ozone loss estimates. Adams, Strong, Zhao, et al. (2012) and Lindenmaier et al. (2012) used data from Eureka with methods similar to this paper. Adams, Strong, Zhao, et al. (2012) estimated a mean ozone loss of 99-108 DU (27-29%) for 12-20 March (GBS and SAOZ data), while Lindenmaier et al. (2012) estimated 35% for all in-vortex measurements (Bruker FTIR data). The corresponding values for 2011 in this paper are 92-77 DU (26-21%), and 13%, respectively. The large differences are due in part to the updated chemistry and transport in the SLIMCAT simulations used here. Adams, Strong, Zhao, et al. (2012) corrected SLIMCAT passive ozone to December ozonesonde columns, while Lindenmaier et al. (2012) did not implement a correction. Given the updated SLIMCAT simulations, and because of the diversity of methods (and sampling of datasets) used in previous studies, loss estimates presented here are not necessarily directly comparable to the literature. Esti-

mates of ozone loss from the present dataset are therefore a better basis of comparison. Using equivalent periods in March for 2011 and 2020, estimates of absolute loss are generally similar or smaller, while relative loss is greater, in 2020 than in 2011, for all instruments. This is consistent with the peak daily loss results discussed above.

Quantifying overall chemical ozone loss from a single ground station is challenging, given the variability of both vortex location and measurement coverage. For the best estimate, the vortex should be stable, and remain above the station, after chemical ozone destruction ceased. This was not the case in 2011, while the spring of 2020 fits these requirements best among all winters in the measurement record presented here. According to all indicators (trace gas measurements, correlation of ozone with temperature, SLIMCAT simulations), ozone depletion stopped by late March 2020. The GBS and Brewer instruments measured inside the vortex for the majority of April. Mean ozone loss in April is then a good indicator of overall chemical ozone loss inside the vortex above Eureka. The mean loss calculated from the GBS measurements is 127 DU (31%), while the same value is 111 DU (27%) using measurements from Brewer #69. Some of these differences are likely related to the different viewing geometries, since DOAS path lengths in the 16-20 km altitude region are several times longer than those for direct-sun measurements. Our ozone loss estimate of 111-127 DU (27-31%) is consistent with values of 125-135 DU from Wohltmann et al. (2020) and Grooß and Müller (2020), who also used the passive tracer method, but with different chemical transport models.

4 Conclusions

The unusually cold, strong, and persistent polar vortex in the winter and spring of 2019/2020 created the greatest potential for ozone depletion ever observed in the Arctic. Accordingly, ozone columns across the Arctic reached record lows, surpassing previous records set in 2011. The GBS, SAOZ, Bruker FTIR, Pandora, and Brewer instruments at Eureka, Canada all observed record low ozone columns (187, 221, 240, 222, and 218 DU) in their respective time series. Persistent enhancements of BrO and OClO dSCDs in the GBS dataset indicate that chlorine activation was ongoing until late March, and consistently low HCl and $ClONO_2$ columns from the Bruker FTIR point to heterogeneous chemistry on PSC particles. HNO_3 columns, on the other hand, were not as low as in 2011, and lower stratospheric temperatures were slightly above T_{NAT} for most of the spring. This is consistent with a less denitrified stratosphere above Eureka indicated by the NO_2 measurements. The smallest ozone column values were observed on 16-19 March, coincident with a significant drop in temperatures and HNO_3 columns. CRL measurements indicated the presence of PSCs (at 14-16 km altitude) during the same period. Ozonesondes measured ozone mixing ratios below 0.5 ppmv (with minima below 0.2 ppmv) in the 16-20 km altitude range in late March and throughout April. These values are unprecedented in the Arctic, and are more similar to values commonly observed in the Antarctic ozone hole. While the vortex remained cold and stable throughout April, chlorine activation largely stopped by the end of March, as evidenced by increasing concentrations of chlorine reservoirs and NO_2.

Dynamical contributions to ozone variability must be considered for an accurate assessment of chemical ozone loss. Passive ozone from the SLIMCAT chemical transport model indicates that ozone column values in 2020 would likely have been unusually low even without chemical processing. Ozone columns are usually smaller in cold winters, and Eureka ozone measurements inside the vortex generally show good correlation with lower stratospheric temperature. This relationship, however, was substantially different in 2020 (and in 2011) compared to what is observed for more typical years. This indicates that chemical ozone depletion played an exceptionally large role, and contributed to significant additional ozone loss, in 2020 when compared to compared to typical Arctic winters. Bruker FTIR measurements normalized by HF total columns confirm the major role of chemistry in shaping the 2020 trace gas time series.

Chemical loss inside the vortex was estimated using measurements at Eureka and SLIMCAT simulations of passive ozone. Using consistent datasets for the entire time series, we showed that all instruments observed smaller daily peak absolute loss in 2020 (81-157 DU) than in 2011 (108-176 DU). The absolute loss time series generally overlap, but the daily peaks were higher in 2011. Daily peak relative loss, on the other hand, was greater in 2020 (25-38%) than in 2011 (24-36%) for all instruments. While overall ozone loss is difficult to estimate from a single ground station due to the variable position of the vortex, spring 2020 measurements have good coverage inside the vortex after chemical depletion stopped. Using Brewer and GBS measurements throughout April, the mean chemical ozone loss inside the vortex was estimated to be 111-127 DU (27-31%) over Eureka. As the Arctic stratosphere changes in response to climate change, long-term datasets remain essential for assessing unusual springtime conditions and ozone depletion. The spring of 2020 was exceptional in the context of the 20-year dataset presented here, but similar (or even more extreme) conditions could arise given the large interannual variability of the Arctic vortex and the slow decline of ozone-depleting substances.

Acknowledgments

The 2006-2020 UT-GBS, PEARL-GBS, SAOZ, Bruker FTIR and CRL measurements were made at PEARL by CANDAC. CANDAC has been supported by the Atlantic Innovation Fund/Nova Scotia Research Innovation Trust, Canada Foundation for Innovation, Canadian Foundation for Climate and Atmospheric Sciences (CFCAS), Canadian Space Agency (CSA), Environment and Climate Change Canada (ECCC), Government of Canada International Polar Year funding, Natural Sciences and Engineering Research Council (NSERC), Northern Scientific Training Program (NSTP), Ontario Innovation Trust, Polar Continental Shelf Program, and Ontario Research Fund. Brewer, Pandora, ozonesonde, and radiosonde measurements were made by ECCC (additional thanks to Michael Brohart, Jonathan Davies, Reno Sit, and Sum Chi Lee). The spring 2004-2020 UT-GBS, PEARL-GBS, SAOZ, Bruker FTIR, Brewer, Pandora, CRL, and ozonesonde measurements were also supported by the Canadian Arctic ACE/OSIRIS Validation Campaigns, which were funded by CSA, NSERC, NSTP, and ECCC. Spring 2007 GBS measurements were also supported by the Centre for Global Change Science. The 2001–2003 GBS measurements were supported by CFCAS and NSTP. K. Bognar was partially supported by the NSERC CREATE Training Program in Arctic Atmospheric Science, the Arctic Validation And Training for Atmospheric Research in Space program, funded by CSA, and ECCC's G&C program. SAOZ participation in the campaigns was supported by the Centre National D'Etudes Spatiales. Work carried out at the Jet Propulsion Laboratory, California Institute of Technology was done under contract with the National Aeronautics and Space Administration. The SLIMCAT modelling was supported by the NERC SISLAC project (NE/R001782/1). The model simulations were performed on the UK Archer and Leeds ARC HPC machines.

The authors wish to thank PEARL site manager Pierre Fogal, the CANDAC operators, and the staff at ECCC's Eureka Weather Station for their contributions to data acquisition, logistics, and on-site support. The authors also wish to thank Matthew Bassford, Elham Farahani, Annemarie Fraser, Cristen Adams, and Sophie Tran for their contribution to the GBS measurements, as well as Rodica Lindenmaier, Rebecca Batchelor, Dan Weaver, Joseph Mendonca, Stephanie Conway, Erik Lutsch, Sébastien Roche, and Alistair Duff for their contribution to the Bruker FTIR measurements and retrievals. We thank Manuel Gebetsberger, Daniel Santana Diaz, Martin Tiefengraber and Alexander Cede from the Pandonia Global Network (PGN) and Nader Abuhassan from SciGlob for their technical support of Pandora measurements in Eureka.

Data availability: UT-GBS and PEARL-GBS ozone and NO_2 data, as well as the Bruker FTIR measurements of ozone, HCl, $ClONO_2$, HNO_3, and HF are available from the NDACC database at `http://www.ndaccdemo.org/stations/eureka-canada`. The

SAOZ ozone and NO_2 data can be found at `http://saoz.obs.uvsq.fr/SAOZ_consol_v3.html`. Ozonesonde and Brewer measurements are available on the World Ozone and Ultraviolet Radiation Data Centre (`https://woudc.org/data/explore.php?lang=en`, Station: Eureka (315)). Radiosonde data are available through the University of Wyoming Upper Air Database (`http://weather.uwyo.edu/upperair/sounding.html`, Station Number: 71917). Other datasets, such as the OClO and BrO dSCDs, the HCl (unfiltered) and NO_2 measurements form the Bruker FTIR, the corrected Pandora ozone, the CRL backscatter coefficients, and the SLIMCAT profiles, are available through the Scholars Portal Dataverse (Bognar et al., 2020). MERRA-2 data used for the DMP calculations are available at `https://disc.sci.gsfc.nasa.gov/uui/datasets?keywords=%22MERRA-2%22`.

References

Adams, C., Strong, K., Batchelor, R. L., Bernath, P. F., Brohede, S., Boone, C., ... Zhao, X. (2012). Validation of ACE and OSIRIS Ozone and NO_2 Measurements Using Ground Based Instruments at 80° N. *Atmospheric Measurement Techniques*, *5*(5), 927–953. doi: 10.5194/amt-5-927-2012

Adams, C., Strong, K., Zhao, X., Bassford, M. R., Chipperfield, M. P., Daffer, W., ... Walker, K. A. (2012). Severe 2011 ozone depletion assessed with 11 years of ozone, NO_2, and OClO measurements at 80°N. *Geophysical Research Letters*, *39*(5). doi: 10.1029/2011GL050478

Adams, C., Strong, K., Zhao, X., Bourassa, A. E., Daffer, W. H., Degenstein, D., ... Wohltmann, I. (2013). The spring 2011 final stratospheric warming above Eureka: anomalous dynamics and chemistry. *Atmospheric Chemistry and Physics*, *13*(2), 611–624. doi: 10.5194/acp-13-611-2013

Balis, D., Isaksen, I. S. A., Zerefos, C., Zyrichidou, I., Eleftheratos, K., Tourpali, K., ... Orsolini, Y. (2011). Observed and modelled record ozone decline over the Arctic during winter/spring 2011. *Geophysical Research Letters*, *38*(23). doi: 10.1029/2011GL049259

Batchelor, R. L., Strong, K., Lindenmaier, R., Mittermeier, R. L., Fast, H., Drummond, J. R., & Fogal, P. F. (2009). A new Bruker IFS 125HR FTIR spectrometer for the polar environment atmospheric research laboratory at Eureka, Nunavut, Canada: measurements and comparison with the existing Bomem DA8 spectrometer. *Journal of Atmospheric and Oceanic Technology*, *26*(7), 1328–1340. doi: 10.1175/2009JTECHA1215.1

Bernhard, G. H., Fioletov, V. E., Grooß, J.-U., Ialongo, I., Johnsen, B., Lakkala, K., ... Svendby, T. (2020). Record-Breaking Increases in Arctic Solar Ultraviolet Radiation Caused by Exceptionally Large Ozone Depletion in 2020. *Geophysical Research Letters*, *n/a*(n/a), e2020GL090844. doi: https://doi.org/10.1029/2020GL090844

Bognar, K., Alwarda, R., Strong, K., Chipperfield, M. P., Dhomse, S. S., Drummond, J. R., ... Zhao, X. (2020). *Replication data for: Unprecedented spring 2020 ozone depletion in the context of 20 years of measurements at Eureka, Canada.* Scholars Portal Dataverse. (V1) doi: 10.5683/SP2/OLZ4PK

Bognar, K., Zhao, X., Strong, K., Boone, C. D., Bourassa, A. E., Degenstein, D. A., ... Zou, J. (2019). Updated validation of ACE and OSIRIS ozone and NO_2 measurements in the Arctic using ground-based instruments at Eureka, Canada. *Journal of Quantitative Spectroscopy and Radiative Transfer*, *238*, 106571. doi: 10.1016/j.jqsrt.2019.07.014

Brohede, S., McLinden, C. A., Berthet, G., Haley, C. S., Murtagh, D., & Sioris, C. E. (2007). A stratospheric NO_2 climatology from Odin/OSIRIS limb-scatter measurements. *Canadian Journal of Physics*, *85*(11), 1253–1274. doi: 10.1139/p07-141

Cede, A. (2019, October). Manual for Blick Software Suite 1.7 [Computer software

manual].

Chipperfield, M. P. (2006). New version of the TOMCAT/SLIMCAT off-line chemical transport model: Intercomparison of stratospheric tracer experiments. *Quarterly Journal of the Royal Meteorological Society*, *132*(617), 1179–1203. doi: 10.1256/qj.05.51

Chipperfield, M. P., Dhomse, S. S., Feng, W., McKenzie, R. L., Velders, G. J. M., & Pyle, J. A. (2015). Quantifying the ozone and ultraviolet benefits already achieved by the Montreal Protocol. *Nature communications*, *6*(1), 1–8. doi: 10.1038/ncomms8233

Chipperfield, M. P., & Jones, R. L. (1999). Relative influences of atmospheric chemistry and transport on Arctic ozone trends. *Nature*, *400*(6744), 551–554. doi: 10.1038/22999

Coy, L., Nash, E. R., & Newman, P. A. (1997). Meteorology of the polar vortex: Spring 1997. *Geophysical Research Letters*, *24*(22), 2693-2696. doi: 10.1029/97GL52832

DeLand, M. T., Bhartia, P. K., Kramarova, N., & Chen, Z. (2020). OMPS LP Observations of PSC Variability During the NH 2019-2020 Season. *Geophysical Research Letters*, *47*(20), e2020GL090216. doi: 10.1029/2020GL090216

Dhomse, S. S., Chipperfield, M. P., Feng, W., Ball, W. T., Unruh, Y. C., Haigh, J. D., ... Smith, A. K. (2013). Stratospheric O_3 changes during 2001–2010: the small role of solar flux variations in a chemical transport model. *Atmospheric Chemistry and Physics*, *13*(19), 10113–10123. doi: 10.5194/acp-13-10113-2013

Dhomse, S. S., Feng, W., Montzka, S. A., Hossaini, R., Keeble, J., Pyle, J. A., ... Chipperfield, M. P. (2019). Delay in recovery of the Antarctic ozone hole from unexpected CFC-11 emissions. *Nature communications*, *10*(1), 1–12.

Dunkerton, T. J., & Delisi, D. P. (1986). Evolution of potential vorticity in the winter stratosphere of January-February 1979. *Journal of Geophysical Research: Atmospheres*, *91*(D1), 1199–1208. doi: 10.1029/JD091iD01p01199

Eyring, V., Waugh, D. W., Bodeker, G. E., Cordero, E., Akiyoshi, H., Austin, J., ... Yoshiki, M. (2007). Multimodel projections of stratospheric ozone in the 21^{st} century. *Journal of Geophysical Research: Atmospheres*, *112*(D16). doi: 10.1029/2006JD008332

Feng, W., Chipperfield, M. P., Davies, S., Mann, G. W., Carslaw, K. S., Dhomse, S., ... Santee, M. L. (2011). Modelling the effect of denitrification on polar ozone depletion for Arctic winter 2004/2005. *Atmospheric Chemistry and Physics*, *11*(13), 6559–6573. doi: 10.5194/acp-11-6559-2011

Feng, W., Chipperfield, M. P., Davies, S., von der Gathen, P., Kyrö, E., Volk, C. M., ... Belyaev, G. (2007). Large chemical ozone loss in 2004/2005 Arctic winter/spring. *Geophysical Research Letters*, *34*(9). doi: 10.1029/2006GL029098

Fogal, P. F., LeBlanc, L. M., & Drummond, J. R. (2013). The Polar Environment Atmospheric Research Laboratory (PEARL): sounding the atmosphere at 80° North. *Arctic*, *66*(3), 377–386. doi: 10.2307/23594645

Fraser, A., Adams, C., Drummond, J. R., Goutail, F., Manney, G., & Strong, K. (2009). The Polar Environment Atmospheric Research Laboratory UV–visible Ground-Based Spectrometer: First measurements of O_3, NO_2, BrO, and OClO columns. *Journal of Quantitative Spectroscopy and Radiative Transfer*, *110*(12), 986–1004. doi: 10.1016/j.jqsrt.2009.02.034

Gelaro, R., McCarty, W., Suárez, M. J., Todling, R., Molod, A., Takacs, L., ... Zhao, B. (2017). The modern-era retrospective analysis for research and applications, version 2 (MERRA-2). *Journal of Climate*, *30*(14), 5419–5454. doi: 10.1175/JCLI-D-16-0758.1

GMAO. (2015). MERRA-2 inst3_3d_asm_Nv: 3d,3-Hourly,Instantaneous,Model-Level,Assimilation,Assimilated Meteorological Fields V5.12.4 [Computer software manual]. Greenbelt, MD, USA. (Accessed: 2020/08/01) doi:

10.5067/WWQSXQ8IVFW8

Griffin, D., Walker, K. A., Conway, S., Kolonjari, F., Strong, K., Batchelor, R., ... Weaver, D. (2017). Multi-year comparisons of ground-based and space-borne Fourier transform spectrometers in the high Arctic between 2006 and 2013. *Atmospheric Measurement Techniques*, *10*(9), 3273–3294. doi: 10.5194/amt-10-3273-2017

Griffin, D., Walker, K. A., Wohltmann, I., Dhomse, S. S., Rex, M., Chipperfield, M. P., ... Tarasick, D. (2019). Stratospheric ozone loss in the Arctic winters between 2005 and 2013 derived with ACE-FTS measurements. *Atmospheric Chemistry and Physics*, *19*(1), 577–601. doi: 10.5194/acp-19-577-2019

Grooß, J.-U., & Müller, R. (2020). Simulation of the record Arctic stratospheric ozone depletion in 2020. *Submitted to: Journal of Geophysical Research: Atmospheres*. doi: 10.1002/essoar.10503569.1

Hendrick, F., Pommereau, J.-P., Goutail, F., Evans, R. D., Ionov, D., Pazmino, A., ... Van Roozendael, M. (2011). NDACC/SAOZ UV-visible total ozone measurements: improved retrieval and comparison with correlative ground-based and satellite observations. *Atmospheric Chemistry and Physics*, *11*(12), 5975–5995. doi: 10.5194/acp-11-5975-2011

Herman, J., Cede, A., Spinei, E., Mount, G., Tzortziou, M., & Abuhassan, N. (2009). NO_2 column amounts from ground-based Pandora and MFDOAS spectrometers using the direct-sun DOAS technique: Intercomparisons and application to OMI validation. *Journal of Geophysical Research: Atmospheres*, *114*(D13). doi: 10.1029/2009JD011848

Herman, J., Evans, R., Cede, A., Abuhassan, N., Petropavlovskikh, I., & McConville, G. (2015). Comparison of ozone retrievals from the Pandora spectrometer system and Dobson spectrophotometer in Boulder, Colorado. *Atmospheric Measurement Techniques*, *8*(8), 3407–3418. doi: 10.5194/amt-8-3407-2015

Hersbach, H., Bell, B., Berrisford, P., Hirahara, S., Hor/'anyi, A., Muñoz-Sabater, J., ... Thépaut, J.-N. (2020). The ERA5 global reanalysis. *Quarterly Journal of the Royal Meteorological Society*, *146*(730), 1999-2049. doi: 10.1002/qj.3803

Hommel, R., Eichmann, K.-U., Aschmann, J., Bramstedt, K., Weber, M., von Savigny, C., ... Burrows, J. P. (2014). Chemical ozone loss and ozone mini-hole event during the Arctic winter 2010/2011 as observed by SCIAMACHY and GOME-2. *Atmospheric Chemistry and Physics*, *14*(7), 3247–3276. doi: 10.5194/acp-14-3247-2014

Inness, A., Chabrillat, S., Flemming, J., Huijnen, V., Langenrock, B., Nicolas, J., ... Razinger, M. (2020). The unusual 2020 Arctic ozone hole as seen in the CAMS reanalysis. *Submitted to: Journal of Geophysical Research: Atmospheres*. doi: 10.1002/essoar.10503751.1

Johansson, S., Santee, M. L., Grooß, J.-U., Höpfner, M., Braun, M., Friedl-Vallon, F., ... Woiwode, W. (2019). Unusual chlorine partitioning in the 2015/16 Arctic winter lowermost stratosphere: observations and simulations. *Atmospheric Chemistry and Physics*, *19*(12), 8311–8338. doi: 10.5194/acp-19-8311-2019

Kerr, J. B. (2002). New methodology for deriving total ozone and other atmospheric variables from Brewer spectrophotometer direct sun spectra. *Journal of Geophysical Research: Atmospheres*, *107*(D23), ACH 22-1–ACH 22-17. doi: 10.1029/2001JD001227

Kerzenmacher, T. E., Walker, K. A., Strong, K., Berman, R., Bernath, P. F., Boone, C. D., ... Wu, H. (2005). Measurements of O_3, NO_2 and temperature during the 2004 Canadian Arctic ACE Validation Campaign. *Geophysical Research Letters*, *32*(16), L16S07. doi: 10.1029/2005GL023032

Kuttippurath, J., Godin-Beekmann, S., Lefèvre, K., Nikulin, G., Santee, M. L., & Froidevaux, L. (2012). Record-breaking ozone loss in the Arctic winter

2010/2011: comparison with 1996/1997. *Atmospheric Chemistry and Physics*, *12*(15), 7073–7085. doi: 10.5194/acp-12-7073-2012

Lawrence, Z. D., Manney, G. L., & Wargan, K. (2018). Reanalysis intercomparisons of stratospheric polar processing diagnostics. *Atmospheric Chemistry and Physics*, *18*(18), 13547–13579. doi: 10.5194/acp-18-13547-2018

Lawrence, Z. D., Perlwitz, J., Butler, A. H., Manney, G. L., Newman, P. A., Lee, S. H., & Nash, E. R. (2020). The Remarkably Strong Arctic Stratospheric Polar Vortex of Winter 2020: Links to Record-Breaking Arctic Oscillation and Ozone Loss. *Journal of Geophysical Research: Atmospheres*, *125*(22), e2020JD033271. doi: 10.1029/2020JD033271

Lindenmaier, R., Strong, K., Batchelor, R. L., Chipperfield, M. P., Daffer, W. H., Drummond, J. R., ... Walker, K. A. (2012). Unusually low ozone, HCl, and HNO_3 column measurements at Eureka, Canada during winter/spring 2011. *Atmospheric Chemistry and Physics*, *12*(8), 3821–3835. doi: 10.5194/acp-12-3821-2012

Mankin, W. G., Coffey, M. T., Goldman, A., Schoeberl, M. R., Lait, L. R., & Newman, P. A. (1990). Airborne measurements of stratospheric constituents over the Arctic in the winter of 1989. *Geophysical Research Letters*, *17*(4), 473-476. doi: 10.1029/GL017i004p00473

Manney, G. L., Daffer, W. H., Zawodny, J. M., Bernath, P. F., Hoppel, K. W., Walker, K. A., ... Waters, J. W. (2007). Solar occultation satellite data and derived meteorological products: Sampling issues and comparisons with Aura Microwave Limb Sounder. *Journal of Geophysical Research: Atmospheres*, *112*(D24). doi: 10.1029/2007JD008709

Manney, G. L., Froidevaux, L., Santee, M. L., Zurek, R. W., & Waters, J. W. (1997). MLS observations of Arctic ozone loss in 199697. *Geophysical Research Letters*, *24*(22), 2697-2700. doi: 10.1029/97GL52827

Manney, G. L., Hegglin, M. I., Daffer, W. H., Santee, M. L., Ray, E. A., Pawson, S., ... Walker, K. A. (2011). Jet characterization in the upper troposphere/lower stratosphere (UTLS): applications to climatology and transport studies. *Atmospheric Chemistry and Physics*, *11*(12), 6115–6137. doi: 10.5194/acp-11-6115-2011

Manney, G. L., & Lawrence, Z. D. (2016). The major stratospheric final warming in 2016: dispersal of vortex air and termination of Arctic chemical ozone loss. *Atmospheric Chemistry and Physics*, *16*(23), 15371–15396. doi: 10.5194/acp-16-15371-2016

Manney, G. L., Lawrence, Z. D., Santee, M. L., Read, W. G., Livesey, N. J., Lambert, A., ... Schwartz, M. J. (2015). A minor sudden stratospheric warming with a major impact: Transport and polar processing in the 2014/2015 Arctic winter. *Geophysical Research Letters*, *42*(18), 7808–7816. doi: 10.1002/2015GL065864

Manney, G. L., Livesey, N. J., Santee, M. L., Froidevaux, L., Lambert, A., Lawrence, Z., ... Fuller, R. A. (2020). Record-low Arctic stratospheric ozone in 2020: MLS observations of chemical processes and comparisons with previous extreme winters. *Geophysical Research Letters*, *47*(16), e2020GL089063. doi: 10.1029/2020GL089063

Manney, G. L., Santee, M. L., Froidevaux, L., Hoppel, K., Livesey, N. J., & Waters, J. W. (2006). EOS MLS observations of ozone loss in the 20042005 Arctic winter. *Geophysical Research Letters*, *33*(4). doi: 10.1029/2005GL024494

Manney, G. L., Santee, M. L., Rex, M., Livesey, N. J., Pitts, M. C., Veefkind, P., ... Zinoviev, N. S. (2011). Unprecedented Arctic ozone loss in 2011. *Nature*, *478*(7370), 469–475. doi: 10.1038/nature10556

Manney, G. L., Zurek, R. W., O'Neill, A., & Swinbank, R. (1994). On the Motion of Air through the Stratospheric Polar Vortex. *Journal of the Atmospheric Sciences*, *51*(20), 2973–2994. doi: 10.1175/1520-0469(1994)051$\langle$\$2973:

OTMOAT$\rangle$2.0.CO;2

Marsh, D. R., Mills, M. J., Kinnison, D. E., Lamarque, J.-F., Calvo, N., & Polvani, L. M. (2013). Climate change from 1850 to 2005 simulated in CESM1 (WACCM). *Journal of climate*, *26*(19), 7372–7391. doi: 10.1175/JCLI-D-12-00558.1

Matthias, V., Dörnbrack, A., & Stober, G. (2016). The extraordinarily strong and cold polar vortex in the early northern winter 2015/2016. *Geophysical Research Letters*, *43*(23), 12,287-12,294. doi: 10.1002/2016GL071676

McCullough, E. M., Drummond, J. R., & Duck, T. J. (2019). Lidar measurements of thin laminations within Arctic clouds. *Atmospheric Chemistry and Physics*, *19*(7), 4595–4614. doi: 10.5194/acp-19-4595-2019

McCullough, E. M., Sica, R. J., Drummond, J. R., Nott, G., Perro, C., Thackray, C. P., ... Walker, K. A. (2017). Depolarization calibration and measurements using the CANDAC Rayleigh–Mie–Raman lidar at Eureka, Canada. *Atmospheric Measurement Techniques*, *10*(11), 4253–4277. doi: 10.5194/amt-10-4253-2017

McElroy, M. B., Salawitch, R. J., Wofsy, S. C., & Logan, J. A. (1986). Reductions of Antarctic ozone due to synergistic interactions of chlorine and bromine. *Nature*, *321*(6072), 759–762. doi: 10.1038/321759a0

McLinden, C. A., Olsen, S. C., Hannegan, B., Wild, O., Prather, M. J., & Sundet, J. (2000). Stratospheric ozone in 3-D models: A simple chemistry and the cross-tropopause flux. *Journal of Geophysical Research: Atmospheres*, *105*(D11), 14653–14665. doi: 10.1029/2000JD900124

Molina, L. T., & Molina, M. J. (1987). Production of chlorine oxide (Cl_2O_2) from the self-reaction of the chlorine oxide (ClO) radical. *Journal of Physical Chemistry*, *91*(2), 433–436. doi: 10.1021/j100286a035

Newman, P. A., Gleason, J. F., McPeters, R. D., & Stolarski, R. S. (1997). Anomalously low ozone over the Arctic. *Geophysical Research Letters*, *24*(22), 2689-2692. doi: 10.1029/97GL52831

Nott, G. J., Duck, T. J., Doyle, J. G., Coffin, M. E. W., Perro, C., Thackray, C. P., ... Sica, R. J. (2012). A remotely operated lidar for aerosol, temperature, and water vapor profiling in the High Arctic. *Journal of Atmospheric and Oceanic Technology*, *29*(2), 221–234. doi: 10.1175/JTECH-D-11-00046.1

Platt, U., & Stutz, J. (2008). *Differential Optical Absorption Spectroscopy*. Springer.

Pommereau, J. P., & Goutail, F. (1988). O_3 and NO_2 ground-based measurements by visible spectrometry during Arctic winter and spring 1988. *Geophysical Research Letters*, *15*(8), 891–894. doi: 10.1029/GL015i008p00891

Pommereau, J.-P., Goutail, F., Lefèvre, F., Pazmino, A., Adams, C., Dorokhov, V., ... van Roozendael, M. (2013). Why unprecedented ozone loss in the Arctic in 2011? Is it related to climate change? *Atmospheric Chemistry and Physics*, *13*(10), 5299–5308. doi: 10.5194/acp-13-5299-2013

Pougatchev, N. S., Connor, B. J., & Rinsland, C. P. (1996). Infrared measurements of the ozone vertical distribution above Kitt Peak. *Journal of Geophysical Research: Atmospheres*, *100*(D8), 16689–16697. doi: 10.1029/95JD01296

Rex, M., Salawitch, R. J., Deckelmann, H., von der Gathen, P., Harris, N. R. P., Chipperfield, M. P., ... Zerefos, C. (2006). Arctic winter 2005: Implications for stratospheric ozone loss and climate change. *Geophysical Research Letters*, *33*(23). doi: 10.1029/2006GL026731

Rex, M., Salawitch, R. J., von der Gathen, P., Harris, N. R. P., Chipperfield, M. P., & Naujokat, B. (2004). Arctic ozone loss and climate change. *Geophysical Research Letters*, *31*(4). doi: 10.1029/2003GL018844

Rodgers, C. D. (2000). *Inverse Methods for Atmospheric Sounding: Theory and Practice* (Vol. 2). World Scientific.

Rothman, L. S., Gordon, I. E., Barbe, A., Benner, D. C., Bernath, P. F., Birk, M., ... Vander Auwera, J. (2009). The HITRAN 2008 molecular spectroscopic

database. *Journal of Quantitative Spectroscopy and Radiative Transfer*, *110*(9-10), 533–572. doi: 10.1016/j.jqsrt.2009.02.013

Salawitch, R. J., Gobbi, G. P., Wofsy, S. C., & McElroy, M. B. (1989). Denitrification in the Antarctic stratosphere. *Nature*, *339*(6225), 525–527. doi: 10.1038/339525a0

Salby, M. L., & Callaghan, P. F. (2007). On the wintertime increase of Arctic ozone: Relationship to changes of the polar-night vortex. *Journal of Geophysical Research: Atmospheres*, *112*(D6). doi: 10.1029/2006JD007948

Singleton, C. S., Randall, C. E., Chipperfield, M. P., Davies, S., Feng, W., Bevilacqua, R. M., ... Harvey, V. L. (2005). 2002-2003 Arctic ozone loss deduced from POAM III satellite observations and the SLIMCAT chemical transport model. *Atmospheric Chemistry and Physics*, *5*(3), 597–609. doi: 10.5194/acp-5-597-2005

Singleton, C. S., Randall, C. E., Harvey, V. L., Chipperfield, M. P., Feng, W., Manney, G. L., ... Hoppel, K. W. (2007). Quantifying Arctic ozone loss during the 20042005 winter using satellite observations and a chemical transport model. *Journal of Geophysical Research: Atmospheres*, *112*(D7). doi: 10.1029/2006JD007463

Sinnhuber, B.-M., Stiller, G., Ruhnke, R., von Clarmann, T., Kellmann, S., & Aschmann, J. (2011). Arctic winter 2010/2011 at the brink of an ozone hole. *Geophysical Research Letters*, *38*(24). doi: 10.1029/2011GL049784

Solomon, S., Garcia, R. R., Rowland, F. S., & Wuebbles, D. J. (1986). On the depletion of Antarctic ozone. *Nature*, *321*(6072), 755–758. doi: 10.1038/321755a0

Solomon, S., Haskins, J., Ivy, D. J., & Min, F. (2014). Fundamental differences between Arctic and Antarctic ozone depletion. *Proceedings of the National Academy of Sciences*, *111*(17), 6220–6225. doi: 10.1073/pnas.1319307111

Strahan, S. E., Douglass, A. R., & Newman, P. A. (2013). The contributions of chemistry and transport to low arctic ozone in March 2011 derived from Aura MLS observations. *Journal of Geophysical Research: Atmospheres*, *118*(3), 1563-1576. doi: 10.1002/jgrd.50181

Tarasick, D. W., Davies, J., Smit, H. G. J., & Oltmans, S. J. (2016). A re-evaluated Canadian ozonesonde record: measurements of the vertical distribution of ozone over Canada from 1966 to 2013. *Atmospheric Measurement Techniques*, *9*(1), 195–214. doi: 10.5194/amt-9-195-2016

Tegtmeier, S., Rex, M., Wohltmann, I., & Krüger, K. (2008). Relative importance of dynamical and chemical contributions to Arctic wintertime ozone. *Geophysical Research Letters*, *35*(17). doi: 10.1029/2008GL034250

Tilmes, S., Müller, R., Engel, A., Rex, M., & Russell III, J. M. (2006). Chemical ozone loss in the Arctic and Antarctic stratosphere between 1992 and 2005. *Geophysical Research Letters*, *33*(20). doi: 10.1029/2006GL026925

Toon, G. C., Farmer, C. B., Schaper, P. W., Lowes, L. L., Norton, R. H., Schoeberl, M. R., ... Newman, P. A. (1992). Evidence for subsidence in the 1989 Arctic winter stratosphere from airborne infrared composition measurements. *Journal of Geophysical Research: Atmospheres*, *97*(D8), 7963-7970. doi: 10.1029/91JD03115

Tung, K.-K., Ko, M. K. W., Rodriguez, J. M., & Sze, N. D. (1986). Are Antarctic ozone variations a manifestation of dynamics or chemistry? *Nature*, *322*(6082), 811–814. doi: 10.1038/322811a0

Tzortziou, M., Herman, J. R., Cede, A., & Abuhassan, N. (2012). High precision, absolute total column ozone measurements from the Pandora spectrometer system: Comparisons with data from a Brewer double monochromator and Aura OMI. *Journal of Geophysical Research: Atmospheres*, *117*(D16). doi: 10.1029/2012JD017814

WMO. (1957). Meteorology – A three-dimensional science: Second session of the commission for aerology. *WMO Bulletin*, *4*(4), 134–138.

WMO. (2014). *Scientific Assessment of Ozone Depletion: 2014.* Geneva, Switzerland: Global Ozone Research and Monitoring Project Report 55.

WMO. (2018). *Scientific Assessment of Ozone Depletion: 2018.* Geneva, Switzerland: Global Ozone Research and Monitoring Project Report 58.

Wohltmann, I., von der Gathen, P., Lehmann, R., Maturilli, M., Deckelmann, H., Manney, G. L., ... Rex, M. (2020). Near-Complete Local Reduction of Arctic Stratospheric Ozone by Severe Chemical Loss in Spring 2020. *Geophysical Research Letters*, *47*(20), e2020GL089547. doi: 10.1029/2020GL089547

Zhao, X., Fioletov, V., Brohart, M., Savastiouk, V., Abboud, I., Ogyu, A., ... McLinden, C. (2020). The world Brewer reference triad–updated performance assessment and new double triad. *Atmospheric Measurement Techniques Discussions*, 1–34. doi: 10.5194/amt-2020-324

Zhao, X., Fioletov, V., Cede, A., Davies, J., & Strong, K. (2016). Accuracy, precision, and temperature dependence of Pandora total ozone measurements estimated from a comparison with the Brewer triad in Toronto. *Atmospheric Measurement Techniques*, *9*(12), 5747–5761. doi: 10.5194/amt-9-5747-2016

Zhao, X., Strong, K., Adams, C., Schofield, R., Yang, X., Richter, A., ... Koo, J.-H. (2016). A case study of a transported bromine explosion event in the Canadian high arctic. *Journal of Geophysical Research: Atmospheres*, *121*(1), 457–477. doi: 10.1002/2015JD023711

Supporting Information for "Unprecedented spring 2020 ozone depletion in the context of 20 years of measurements at Eureka, Canada"

Kristof Bognar[1], Ramina Alwarda[1], Kimberly Strong[1], Martyn P. Chipperfield[2,3], Sandip Dhomse[2,3], James R. Drummond[4], Wuhu Feng[2,5], Vitali Fioletov[6], Florence Goutail[7], Beatriz Herrera[1], Gloria L. Manney[8,9], Emily M. McCullough[4], Luis F. Millán[10], Andrea Pazmino[7], Kaley A. Walker[1], Tyler Wizenberg[1], Xiaoyi Zhao[6]

[1]Department of Physics, University of Toronto, Toronto, ON, Canada

[2]School of Earth and Environment, University of Leeds, Leeds, UK

[3]National Centre for Earth Observation, University of Leeds, Leeds, UK

[4]Department of Physics and Atmospheric Science, Dalhousie University, Halifax, NS, Canada

[5]National Centre for Atmospheric Science, University of Leeds, Leeds, UK

[6]Air Quality Research Division, Environment and Climate Change Canada, Toronto, ON, Canada

[7]LATMOS/IPSL, UVSQ Université Paris-Saclay, Sorbonne Université, CNRS, Guyancourt, France

[8]NorthWest Research Associates, Socorro, NM, USA

[9]Department of Physics, New Mexico Institute of Mining and Technology, Socorro, NM, USA

[10]Jet Propulsion Laboratory, California Institute of Technology, Pasadena, CA, USA

Corresponding author: K. Bognar, Department of Physics, University of Toronto, Toronto, ON, Canada. (kbognar@atmosp.physics.utoronto.ca)

Corresponding author: K. Strong, Department of Physics, University of Toronto, Toronto, ON,

Contents of this file

1. Text S1 to S2

2. Figures S1 to S5

Introduction

• Text S1 describes the normalization of Bruker FTIR measurements with the HF total columns.

• Text S2 describes the comparisons SLIMCAT trace gas columns with measured values.

• Figure S1 shows the HF columns from the Bruker FTIR, as well as the normalized time series of ozone, NO_2, HCl, $ClONO_2$, and HNO_3.

• Figure S2 shows the absolute differences between SLIMCAT active ozone and ozone measurements from the GBS, SAOZ, Bruker FTIR, and Brewer instruments.

• Figure S3 shows the relative differences between SLIMCAT active ozone and ozone measurements from the GBS, SAOZ, Bruker FTIR, and Brewer instruments.

• Figure S4 shows the absolute differences between SLIMCAT HCl, $ClONO_2$, and HNO_3, and the Bruker FTIR measurements.

• Figure S5 shows the relative differences between SLIMCAT HCl, $ClONO_2$, and HNO_3, and the Bruker FTIR measurements.

Canada. (strong@atmosp.physics.utoronto.ca)

Text S1. Normalizing with HF

The Bruker FTIR HF retrievals use the same settings (following NDACC recommendations) as described for the other trace gases in the main text. The mean uncertainty of the HF columns for the measurement period is 3.5%, and the mean DOFS is 2.8. We use the HF columns as a tracer of vertical motion in the vortex (after Lindenmaier et al., 2012). HF displays a significant increasing trend in the Arctic stratosphere (e.g. Griffin et al., 2017), likely due to an increase in its source gases. To estimate the HF trend for the Bruker FTIR, we calculated yearly averages of HF columns outside the vortex (after Griffin et al., 2017), using the vortex criteria described in the main text. The yearly averages were then fitted using a robust fitting method, as described in Bognar et al. (2019). The line of best fit indicates a statistically significant increase of 4.33 ± 2.46 molec cm^{-1} yr^{-1} (2.1 ± 1.2 % yr^{-1} relative to 2007) in the yearly mean HF columns for 2007-2019 (no out-of-vortex measurements in 2020). To correct for this trend, the line of best fit (yearly values) was subtracted from all HF data, using 2007 as the baseline.

To remove the impact of some of the dynamical effects, we normalized trace gas column with the nearest trend-corrected HF measurement (within a $\pm$2 hour time window). The time series of HF and the normalized time series of ozone, NO_2, HCl, $ClONO_2$, and HNO_3 are shown in Figure S1, and discussed in the main text. The effect of the trend correction is most evident in the HF time series. Uncorrected HF columns for 2020 are much higher than those in 2011, while the trend-corrected columns are similar for both years. The interpretation of the ratio time series does not change as a function of the trend correction.

Text S2. SLIMCAT comparisons

To compare trace gas columns from SLIMCAT to measured column values, the 6-hourly SLIMCAT output was linearly interpolated to the individual measurement times. For the comparisons, the mean absolute difference was calculated as

$$\Delta_{abs} = \frac{1}{N}\sum_{i=1}^{N}(MODEL_i - MEAS_i), \quad (1)$$

and the mean relative differences were calculated as

$$\Delta_{rel} = \frac{1}{N}\sum_{i=1}^{N}\frac{(MODEL_i - MEAS_i)}{MEAS_i} \times 100\%, \quad (2)$$

where $MEAS_i$ and $MODEL_i$ are the individual measurements and corresponding SLIMCAT values, respectively. The reported uncertainty in the figures and in the text is the standard deviation of the differences. Differences were calculated separately for measurements inside and outside the vortex, using the vortex criteria for the measurements described in the main text. Since the instruments generally look south from Eureka, most measurements that sample inside the vortex correspond to times when the vertical profile directly over Eureka is also inside the vortex. For the ozone loss estimates in 2011 and 2020, vortex criteria were tested explicitly for SLIMCAT columns as well (see main text). In the following we present comparisons of SLIMCAT ozone, HCl, $ClONO_2$, and HNO_3 to GBS, SAOZ, Bruker FTIR and Brewer measurements, using all measurements from each instrument. SLIMCAT simulates OClO, BrO and NO_2 (the other trace gases of interest) as well, but comparison of these results is not straightforward given the large diurnal variation of each trace gas, and the coarse temporal resolution (6 hours) of the SLIMCAT output.

Figures S2 and S3 show absolute and relative differences between SLIMCAT active ozone and measured ozone as a function of time of year and vortex location. SLIM-

CAT generally agrees well with (and slightly underestimates) measurements inside the vortex. The mean relative differences are 1.4%, -3.9%, -8.9%, and -4.0% for the GBS, SAOZ, Bruker FTIR and Brewer data, respectively. The changes in the mean relative differences are consistent with the agreement between the various instruments (Bognar et al., 2019). The SLIMCAT results show the largest deviations when compared to Bruker FTIR measurements in late February. This peak is in large part the consequence of differences in spatial sampling. The SLIMCAT columns correspond to vertical profiles above Eureka, while the Bruker FTIR measurements have ground footprints of hundreds of km in the early spring due to large SZA. The the largest deviations between SLIMCAT and the Bruker FTIR occur for SZA>87°, which is expected given that the Bruker FTIR line-of-sight reaches 16 km altitude (the approximate lower boundary of the peak ozone concentrations) on average 150 km away from Eureka for such large SZA. Excluding measurements with SZA>87° reduces the late February differences, and so the mean relative differences improve to -8.2±3.9%. Comparisons to the GBS and SAOZ datasets do not show significant seasonal differences, likely due to longer stratospheric pathlengths for the ZSL-DOAS measurements. Brewer measurements inside the vortex are mostly restricted to 2020, and so the mean differences should be interpreted with caution.

SLIMCAT active ozone outside the vortex generally overestimates the measurements. A consistent offset of 10-11% (40-45 DU) is apparent between inside and outside comparisons across all instruments. Comparisons to Microwave Limb Sounder (MLS, on board NASA's Aura satellite) data indicate that this difference is already present at the start of the winter. The difference is likely related to model dynamics, and not to the springtime ozone depletion chemistry.

Figures S4 and S5 show absolute and relative differences between SLIMCAT HCl, $ClONO_2$, and HNO_3 and Bruker FTIR measurements, as a function of time of year and vortex location. HCl comparisons show similarly good agreement inside and outside the vortex, but with a significant early-season slope in the in-vortex differences. This is largely the result of the sampling issues discussed above. Excluding Bruker FTIR measurements with SZA>87°, the comparisons inside the vortex improve to -1.8% (from -4.0% when including all measurements). Measurement SZA does not have a significant impact on comparisons outside the vortex, likely because of the more uniform HCl background (Fig. 2c in the main text). $ClONO_2$ comparisons indicate very good agreement inside the vortex (0.6%), while SLIMCAT significantly overestimates $ClONO_2$ outside the vortex. It should be noted that $ClONO_2$ columns outside the vortex are generally small (Fig. 2d in the main text), and so the relative differences are large. $ClONO_2$ differences appear related to lower stratospheric temperature, with increasing differences for increasing temperatures (slope of $\sim$1.1% K^{-1} for differences inside the vortex). SLIMCAT generally underestimates HNO_3 both inside and outside the vortex (by 18.2% and 11.0%, respectively). This is expected given the simple equilibrium denitrification scheme included in the model. The scatter in the differences increases as temperatures approach T_{NAT}. The large spike in the comparisons around 18 March corresponds to the record low HNO_3 columns measured by the Bruker FTIR in 2020 (Fig. 2e in the main text).

The SLIMCAT comparisons presented here are in broad agreement with Lindenmaier et al. (2012), who compared SLIMCAT data to Bruker FTIR measurements for 2011. The differences between measurements inside and outside the vortex are consistent, and the underestimation of HNO_3 is present in both studies. Direct comparisons are difficult,

however, since the model simulations in Lindenmaier et al. (2012) used an older version of SLIMCAT, with lower resolution and different reanalysis input.

References

Bognar, K., Zhao, X., Strong, K., Boone, C. D., Bourassa, A. E., Degenstein, D. A., ... Zou, J. (2019). Updated validation of ACE and OSIRIS ozone and NO_2 measurements in the Arctic using ground-based instruments at Eureka, Canada. *Journal of Quantitative Spectroscopy and Radiative Transfer*, *238*, 106571. doi: 10.1016/j.jqsrt.2019.07.014

Griffin, D., Walker, K. A., Conway, S., Kolonjari, F., Strong, K., Batchelor, R., ... Weaver, D. (2017). Multi-year comparisons of ground-based and space-borne Fourier transform spectrometers in the high Arctic between 2006 and 2013. *Atmospheric Measurement Techniques*, *10*(9), 3273–3294. doi: 10.5194/amt-10-3273-2017

Lindenmaier, R., Strong, K., Batchelor, R. L., Chipperfield, M. P., Daffer, W. H., Drummond, J. R., ... Walker, K. A. (2012). Unusually low ozone, HCl, and HNO_3 column measurements at Eureka, Canada during winter/spring 2011. *Atmospheric Chemistry and Physics*, *12*(8), 3821–3835. doi: 10.5194/acp-12-3821-2012

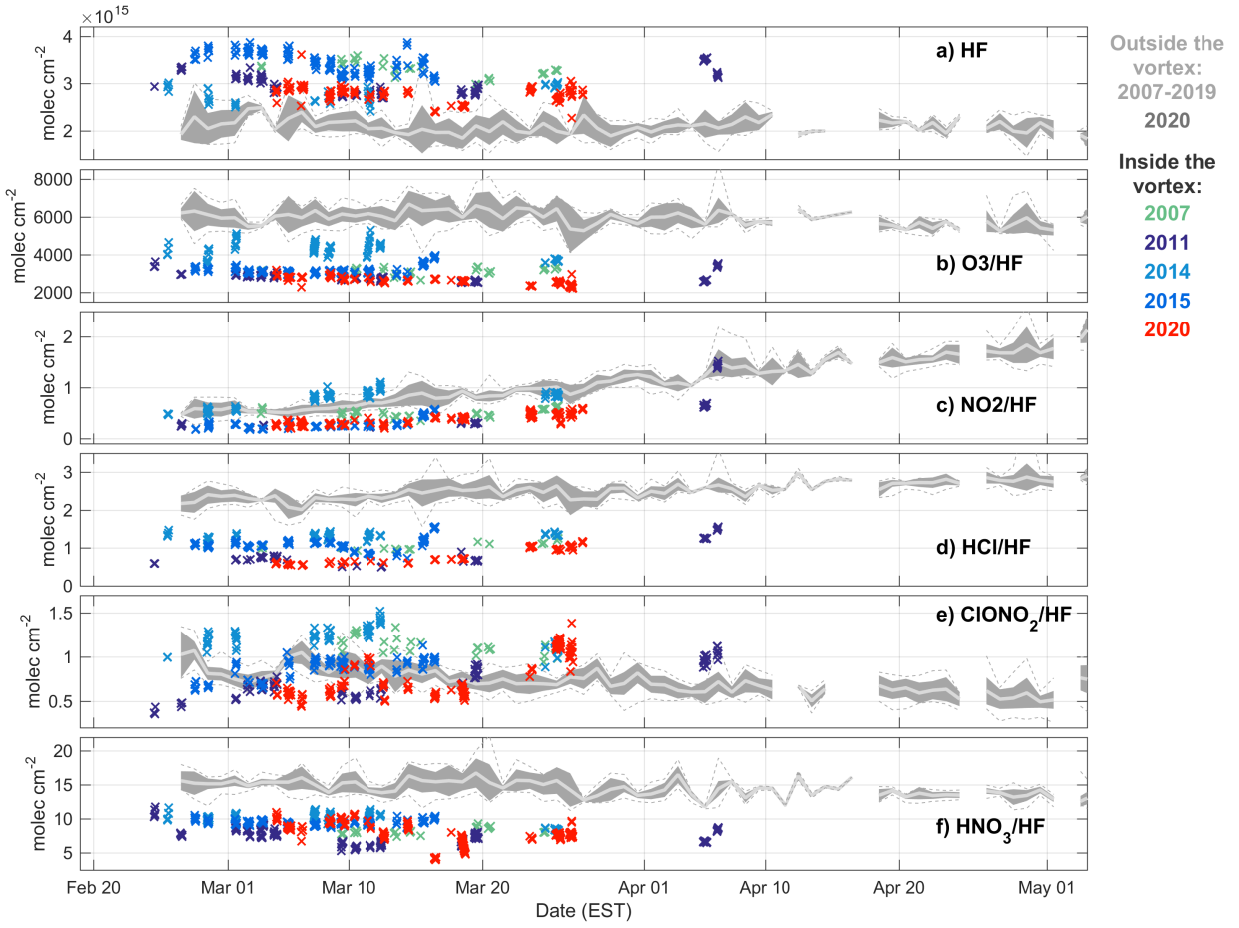

Figure S1. **a)** Measurements of HF columns from the Bruker FTIR. Measurements of **b)** ozone, **c)** NO_2, **d)** HCl, **e)** $ClONO_2$, and **f)** HNO_3, normalized by the HF columns. NO_2 columns were scaled to local noon prior to normalization. Measurements outside the vortex (up to 2019) are represented by the gray shaded area (daily mean and standard deviation) and the gray dashed lines (daily minima and maxima). The colored datapoints represent measurements inside the vortex, in years when the vortex was located above Eureka for a substantial part of the measurement period.

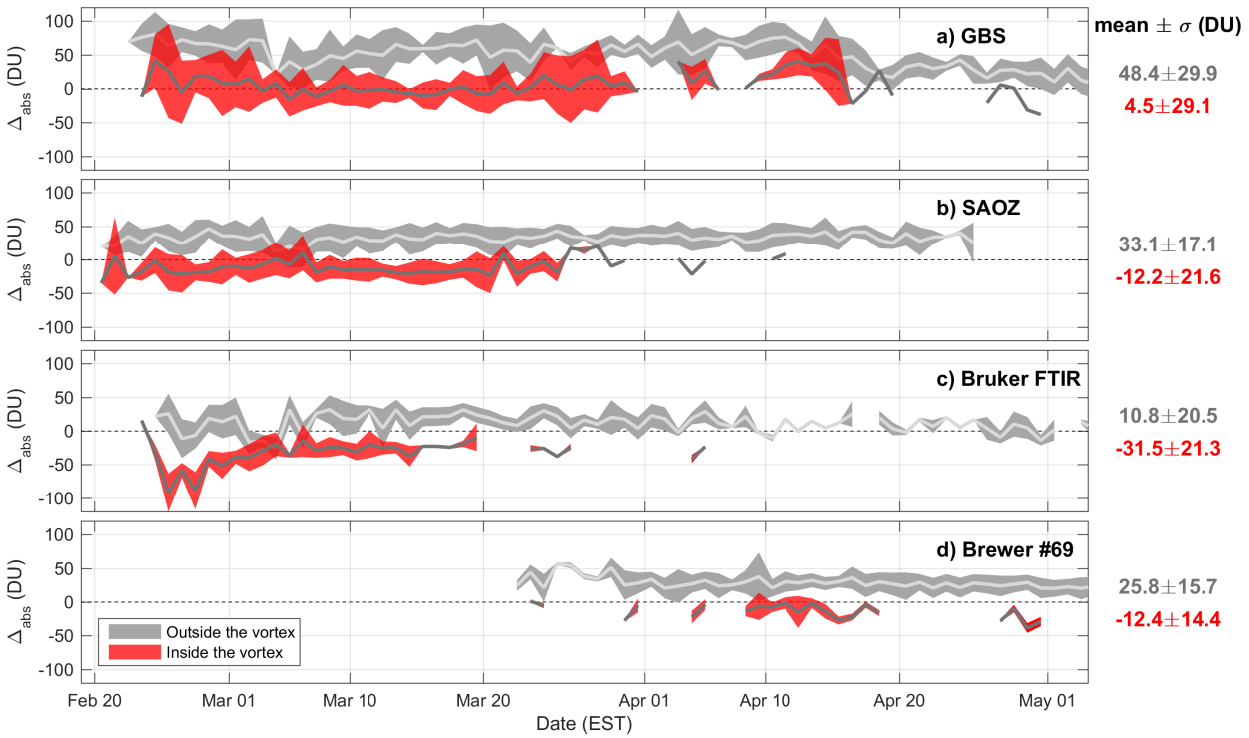

Figure S2. Absolute differences between SLIMCAT active ozone and measurements of ozone from **a)** GBS, **b)** SAOZ, **c)** Bruker FTIR and **d)** Brewer instruments, for all years with available data. The solid lines and shaded areas show daily mean and corresponding standard deviation from all available years. Measurements inside the vortex are shown by the red shading, while out-of-vortex measurements are shown in gray. Standard deviations are only plotted if more than two measurements are available for the given day. The overall mean absolute differences (and corresponding standard deviations) are indicated on the right for measurements inside and outside the vortex.

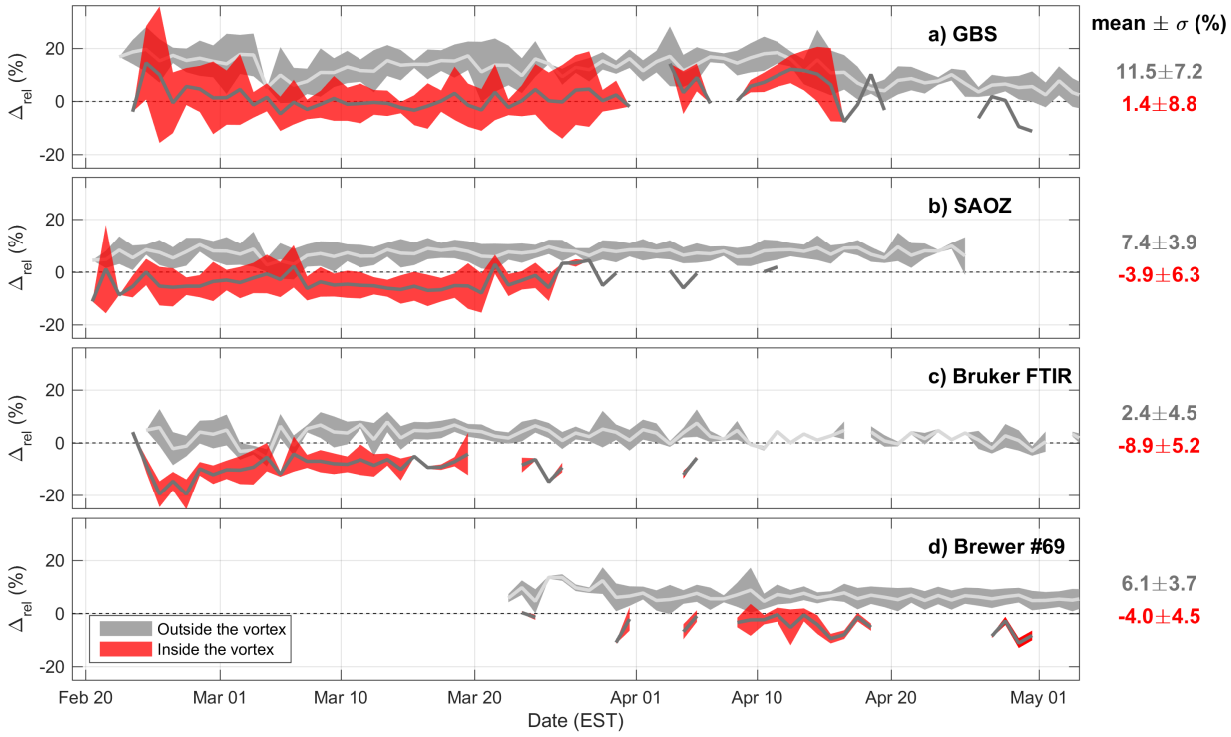

Figure S3. As for Figure S2, with relative ozone differences.

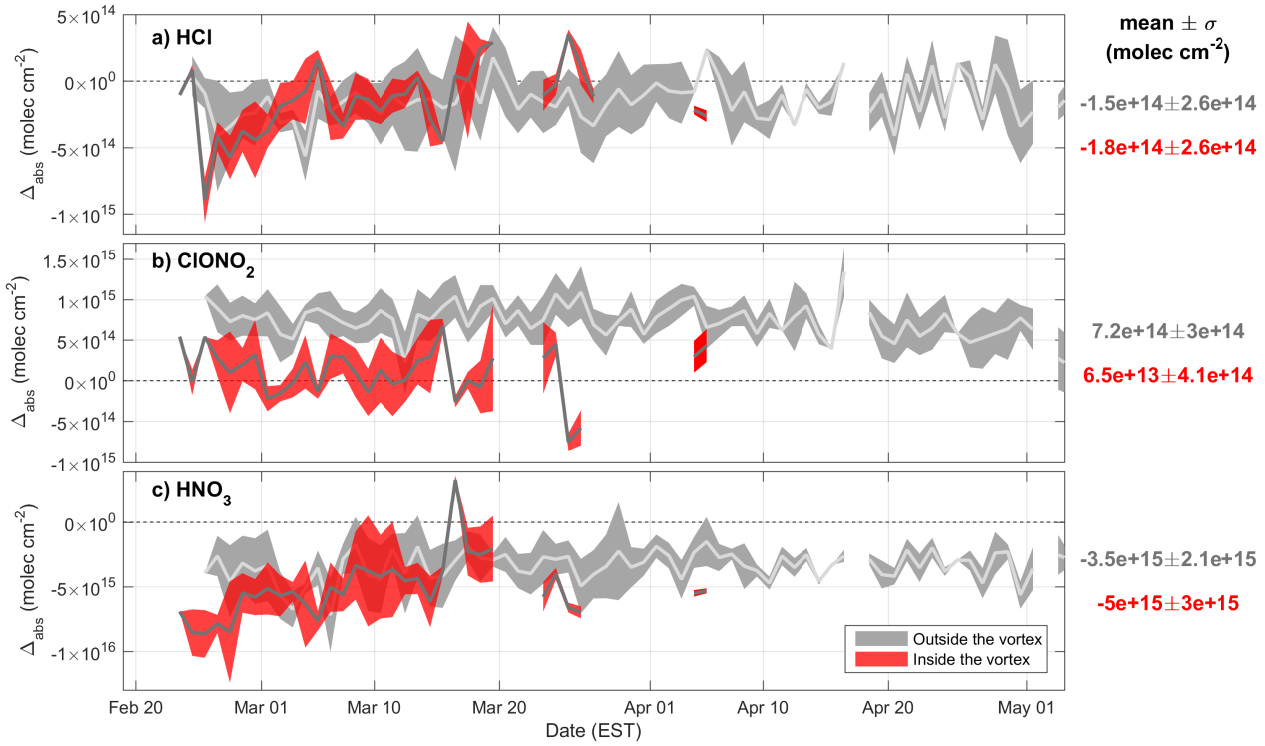

Figure S4. As for Figure S2, with SLIMCAT vs Bruker FTIR absolute differences for **a)** HCl, **b)** $ClONO_2$, and **c)** HNO_3. Note that the y-axis limits are different for each trace gas.

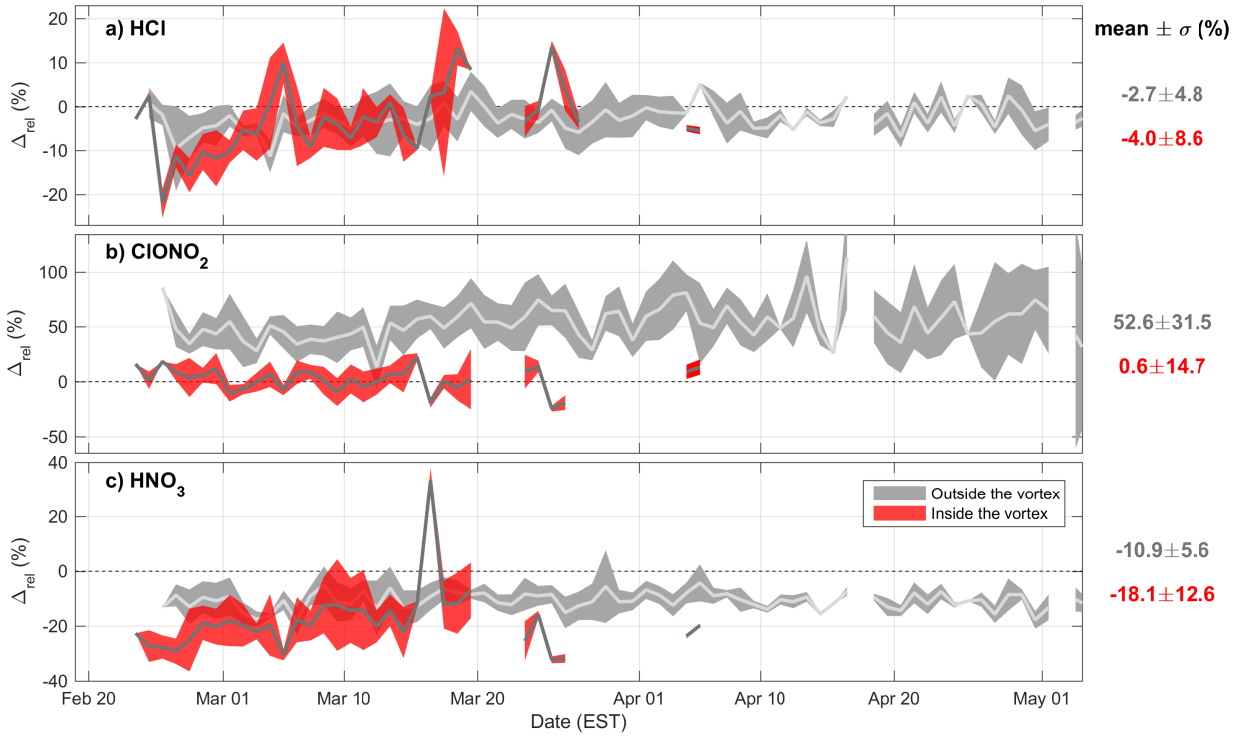

Figure S5. As for Figure S2, with SLIMCAT vs Bruker FTIR relative differences for **a)** HCl, **b)** $ClONO_2$, and **c)** HNO_3. Note that the y-axis limits are different for each trace gas.